Chemical Geology 254 (2008) 19–35

Contents lists available at ScienceDirect

Chemical Geology

journal homepage: www.elsevier.com/locate/chemgeo

Sr- and Nd-isotope geochemistry of the Atlantis Massif (30°N, MAR): Implications for fluid fluxes and lithospheric heterogeneity

Adélie Delacour [a,*], Gretchen L. Früh-Green [a], Martin Frank [b,c], Marcus Gutjahr [c], Deborah S. Kelley [d]

[a] Institute for Mineralogy and Petrology, ETH Zurich, CH-8092 Zurich, Switzerland
[b] IFM-Geomar, Leibniz Institute for Marine Sciences, 24148 Kiel, Germany
[c] Institute of Isotope Geology and Mineral Resources, ETH Zurich, CH-8092 Zurich, Switzerland
[d] School of Oceanography, University of Washington, Seattle, WA 98195, USA

ARTICLE INFO

Article history:
Received 19 July 2007
Received in revised form 14 February 2008
Accepted 26 May 2008

Editor: R.L. Rudnick

Keywords:
Fluid fluxes
Water–rock ratios
Radiogenic isotopes
Serpentinites
Atlantis Massif
Lost City

ABSTRACT

The Atlantis Massif (Mid-Atlantic Ridge, 30°N) is an oceanic core complex marked by distinct variations in crustal architecture, deformation and metamorphism over distances of at least 5 km. We report Sr and Nd isotope data and Rare Earth Element (REE) concentrations of gabbroic and ultramafic rocks drilled at the central dome (IODP Hole 1309D) and recovered by submersible from the southern ridge of the massif that underlie the peridotite-hosted Lost City Hydrothermal Field. Systematic variations between the two areas document variations in seawater penetration and degree of fluid–rock interaction during uplift and emplacement of the massif and hydrothermal activity associated with the formation of Lost City. Homogeneous Sr and Nd isotope compositions of the gabbroic rocks from the two areas ($^{87}Sr/^{86}Sr$: 0.70261–0.70429 and ε_{Nd}: +9.1 to +12.1) indicate an origin from a depleted mantle. At the central dome, serpentinized peridotites are rare and show elevated seawater-like Sr isotope compositions related to serpentinization at shallow crustal levels, whereas unaltered mantle isotopic compositions preserved in the gabbroic rocks attest to limited seawater interaction at depth. This portion of the massif remained relatively unaffected by Lost City hydrothermal activity. In contrast, pervasive alteration and seawater-like Sr and Nd isotope compositions of serpentinites at the southern wall ($^{87}Sr/^{86}Sr$: 0.70885–0.70918; ε_{Nd}: −4.7 to +11.3) indicate very high fluid–rock ratios (~20 and up to 10^6) and enhanced fluid fluxes during hydrothermal circulation. Our studies show that Nd isotopes are most sensitive to high fluid fluxes and are thus an important geochemical tracer for quantification of water–rock ratios in hydrothermal systems. Our results suggest that high fluxes and long-lived serpentinization processes may be critical to the formation of Lost City-type systems and that normal faulting and mass wasting in the south facilitate seawater penetration necessary to sustain hydrothermal activity.

1. Introduction

The penetration, circulation and interaction of seawater with basalts, gabbros and/or peridotites in mid-ocean ridge environments is a first order process that leads to the release and/or uptake of elements (e.g., Si, Mg, Na, S, B, volatiles) and determines mass transfer between geochemical reservoirs. Fluid–rock interaction has important consequences for geochemical cycles in the oceans as well as for elemental fluxes during dehydration of altered oceanic crust in subduction zones, and in turn influences the chemical variability of the overlying mantle wedge. Numerous studies have documented chemical exchange and mineralogical changes during seawater interaction with the volcanic section, sheeted dykes and plutonic section of the oceanic crust (e.g., Hart, 1970; Humphris and Thompson, 1978a,b; Ludden and Thompson, 1979; Kempton et al., 1991; Stakes et al., 1991; Alt, 1995; Hart et al., 1999; Bach et al., 2001; Alt, 2003, 2004; Alt and Bach, 2006; Gao et al., 2006) and in obducted ophiolite complexes (e.g., Troodos; Spooner et al., 1977; Kawahata and Scott, 1990; Gillis et al., 1992). Sr isotope compositions have proven an important geochemical tool to quantify fluid–rock interaction in these environments (Dasch et al., 1973; Hart et al., 1974; Spooner et al., 1977; Jacobsen and Wasserburg, 1979; Menzies and Seyfried, 1979; McCulloch et al., 1980; Hess et al., 1991; Kempton et al., 1991; Bickle and Teagle, 1992; Hart et al., 1999; Gillis et al., 2005); however, fewer studies address chemical and mineralogical changes during seawater–peridotite interaction in present-day oceanic environments (Bonatti et al., 1970; Kempton and Stephens, 1997; Mével, 2003; Bach et al., 2004; Früh-Green et al., 2004; Bach et al., 2006; Boschi et al., 2006; Paulick et al., 2006). Studies that quantify fluid fluxes with Sr isotope data from serpentinites are limited to ophiolite complexes and Nd isotope data on serpentinized peridotites are particularly rare (Snow et al., 1994; Salters and Dick, 2002; Cipriani et al., 2004).

The Atlantis Massif (AM; Fig. 1) is an ideal site to study the influence of seawater–peridotite and seawater–gabbro interaction linked to the

* Corresponding author. Present address: Laboratoire de Géosciences Marines, Institut de Physique du Globe de Paris, 4 place Jussieu, 75252 Paris Cedex 5, France. Tel.: +33 1 44 27 46 01; fax: +33 1 44 27 99 69.
E-mail address: delacour@ipgp.jussieu.fr (A. Delacour).

0009-2541/$ – see front matter © 2008 Elsevier B.V. All rights reserved.
doi:10.1016/j.chemgeo.2008.05.018

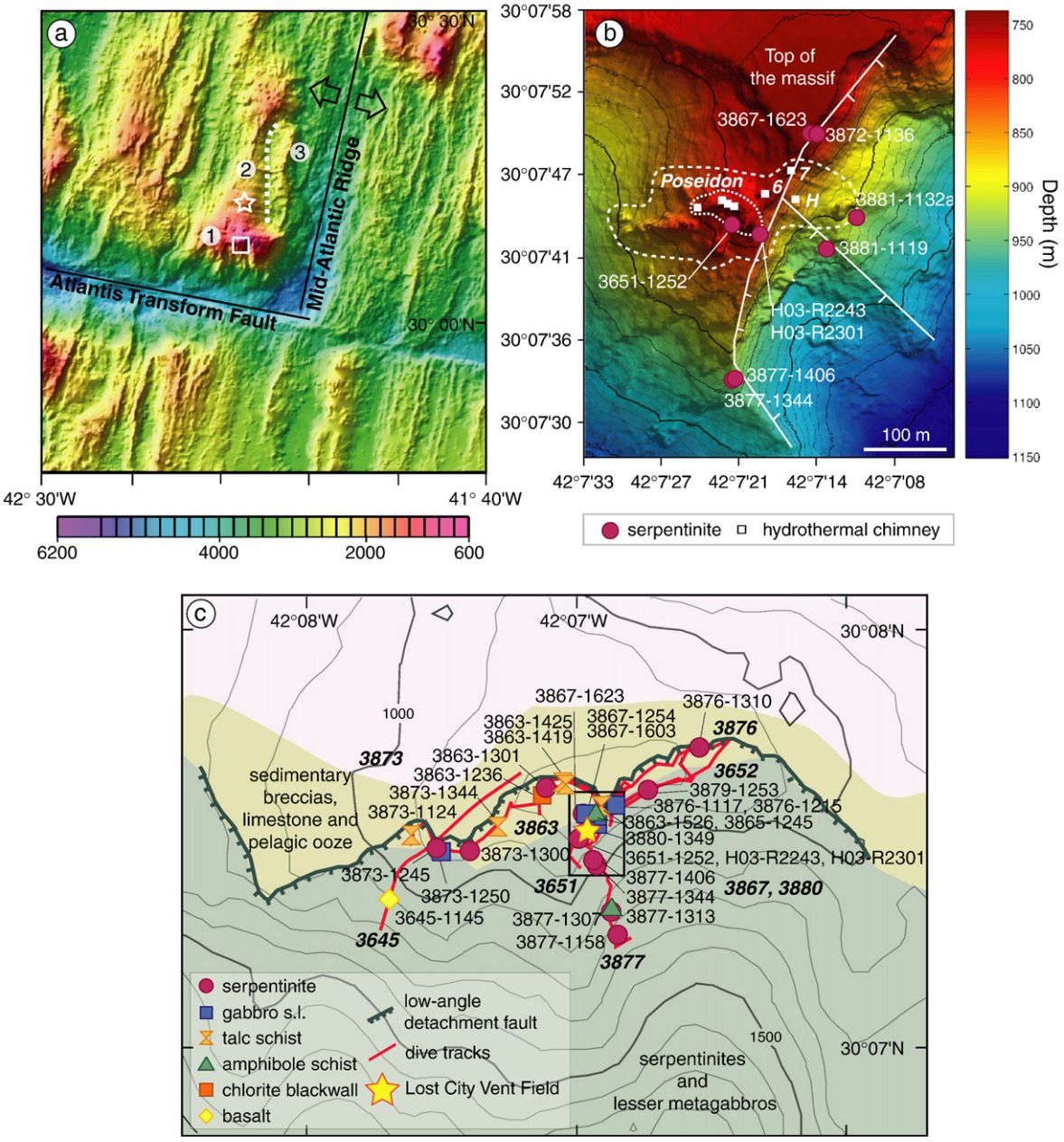

Fig. 1. a. Location map and morphology of the Atlantis Massif (AM) at the inside corner of the intersection between the slow-spreading Mid-Atlantic Ridge and the Atlantis Transform Fault. Based on morphologic and lithologic criteria, the AM is divided into three domains: (1) the peridotite-dominated southern ridge; (2) the gabbroic central dome; and (3) the volcanic eastern block. The white box shows the study area of the southern ridge of the massif and the Lost City Hydrothermal Field (LCHF), enlarged in Fig. 1b and c. White star: Site U1309 investigated during IODP Expeditions 304 and 305. b. High resolution map of LCHF obtained by the autonomous vehicle ABE and gridded at 2 m (Kelley et al., 2005). The external dashed line shows the spatial extent of the active field and major carbonate structures, whereas the internal finely dashed line indicates the base of the largest, 60 m high, hydrothermal structure, Poseidon. The location of the samples investigated in this study are shown relative to the positions of other active structures, identified by field markers 6, H and 7 (shown as solid squares). Locations of normal faults identified by Karson et al. (2006) are shown by the white-hatched lines. c. Simplified geologic map of the top of the southern wall of the Atlantis Massif showing location and lithologies of the samples analyzed in this study and dive tracks (red lines) from the 2000 and 2003 cruises. Green hatched line: trace of the detachment shear zone (DSZ) at the top of the massif (Karson et al., 2006); yellow star: location of the LCHF.

formation of an oceanic core complex (OCC) and to an active peridotite-hosted hydrothermal system. The southern ridge of the massif hosts the Lost City Hydrothermal Field (LCHF), which is driven by serpentinization processes and cooling of underlying mantle peridotites (Kelley et al., 2001, 2005). Interaction of infiltrating seawater with the mantle peridotites influences the chemical compositions of the venting fluids and the newly formed serpentinites and leads to up to 60 m-high towers of hydrothermal carbonate precipitates. Elements such as U, B, and Rare Earth Elements (REE) are enriched in the serpentinites relative to estimated primary compositions, whereas Ca is lost during serpentinization (Früh-Green et al., 2005).

Recent drilling of the Integrated Ocean Drilling Program (IODP) at the central dome of the Atlantis Massif (Fig. 1a) recovered predominantly gabbroic rocks with minor intercalated ultramafic rocks (Expedition Scientific Party, 2005a,b; Blackman et al., 2006) and revealed the heterogeneous nature of the massif over a distance of at least 5 km. Preliminary shipboard results indicate that seawater circulation and high temperature alteration was limited in the central dome and that this portion of the massif remained relatively unaffected by hydrothermal circulation related to the LCHF (Expedition Scientific Party, 2005a,b; Blackman et al., 2006). The gabbroic and ultramafic rocks of the central dome can therefore be regarded as providing "background" compositions

and allow us to better understand and quantify the effects of the Lost City hydrothermal system on the basement rocks of the southern part of the massif.

Changes in chemical composition during hydrothermal alteration are related to the mobility of elements (major, trace and REE) and depend on water–rock ratios, exposure times on the ocean floor (e.g.,

Table 1
Major and trace elements analyses of the serpentinized peridotites and olivine-rich troctolites recovered from Hole 1309D of the central dome of the Atlantis Massif

Leg	304	304	304	304	304	305	305	305	305	305	305
Site	1309B	1309D	1309D	1309D	1309D	1309D	1309D	1309D	1309D	1309D	1309D
Core	11R	27R	42R	58R	65R	232R	234R	237R	241R	248R	256R
Section	1	3	1	1	2	1	2	2	2	1	2
Interval	23–30 cm	6–9 cm	0–8 cm	50–57 cm	22–30 cm	20–31 cm	102–110 cm	7–17 cm	97–108 cm	114–120 cm	46–56 cm
Depth (mbsf)	57.23	155.14	224.3	300.9	335.72	1115.3	1127.22	1140.59	1160.74	1193.04	1231.9
Type of rock	Harzburgite	Harzburgite	Talc-rich harzburgite	Harzburgite	Cr-rich harzburgite	Olivine-rich troctolite	Olivine-rich troctolite	Olivine-rich troctolite	Olivine-rich troctolite	Olivine-rich troctolite	Olivine-rich troctolite
Alteration (%)	90	90	90	70	50	10	10	10	10	5	10
SiO_2	37.96	36.34	44.58	35.87	35.53	38.86	37.63	37.45	38.76	40.11	38.89
Al_2O_3	0.79	0.72	0.63	1.24	1.03	6.39	3.45	4.36	5.62	3.16	3.39
Fe_2O_3	8.16	9.35	8.93	9.77	11.53	10.81	11.89	11.08	11.62	10.25	12.34
MnO	0.076	0.100	0.089	0.109	0.067	0.155	0.167	0.162	0.161	0.179	0.179
MgO	39.77	39.65	34.6	39.94	39.51	32.56	39.35	36.25	36.44	43.41	38.27
CaO	0.27	0.60	0.88	0.09	0.14	4.15	2.23	3.49	3.32	2.02	3.08
Na_2O	0.12	0.05	0.11	0.07	0.07	0.42	0.26	0.20	0.43	0.28	0.25
K_2O	<0.01	0.02	<0.01	<0.01	<0.01	0.04	<0.01	<0.01	0.02	<0.01	<0.01
TiO_2	0.005	0.021	0.04	0.058	0.038	0.06	0.04	0.057	0.043	0.041	0.057
P_2O_5	<0.01	0.01	0.02	0.01	<0.01	0.02	0.01	<0.01	0.01	0.01	<0.01
LOI	12.43	12.92	9.98	12.48	11.99	5.47	4.73	6.55	3.38	<0.01	3.25
Total	99.56	99.80	99.86	99.63	99.83	98.92	99.74	99.57	99.81	99.41	99.67
Trace elements											
Ce	0.24	0.07	0.27	0.18	0.07	0.27	0.17	0.17	0.18	0.15	0.18
Co	111	114	106	116	127	77	109	115	107	58	104
Cr	2190	1910	2110	1930	4420	1230	550	2210	1240	850	1720
Cs (d.l=<0.1 ppm)	<0.1	<d.l.	0.4	0.3	<d.l.	<d.l.	<d.l.	<d.l.	<d.l.	<d.l.	<d.l.
Cu (d.l.=<10 ppm)	<10	20	<d.l.	40	50	40	280	50	50	20	50
Dy	0.02	0.08	0.31	0.23	0.08	0.22	0.12	0.24	0.11	0.11	0.23
Er	0.03	0.05	0.22	0.15	0.06	0.13	0.10	0.15	0.08	0.08	0.16
Eu	0.018	0.011	0.087	0.039	0.024	0.087	0.053	0.068	0.067	0.038	0.065
Ga (d.l.=<1 ppm)	<1	<d.l.	2	1	2	4	2	3	4	2	2
Gd	0.01	0.05	0.21	0.17	0.03	0.15	0.09	0.15	0.07	0.07	0.17
Ge (d.l=<0.5 ppm)	0.9	1.2	2.1	1.2	1.5	0.5	1.2	1.2	0.9	<d.l.	1.1
Hf (d.l=<0.1 ppm)	<0.1	<d.l.	<d.l.	<d.l.	<d.l.	<d.l.	<d.l.	<d.l.	<d.l.	<d.l.	<d.l.
Ho	<0.01	0.02	0.07	0.05	0.02	0.05	0.03	0.05	0.03	0.02	0.05
La	0.07	<0.05	0.08	<d.l.	<d.l.	0.08	<d.l.	<d.l.	0.05	<d.l.	<d.l.
Lu (d.l=<0.05 ppm)	0.009	0.01	0.038	0.024	0.014	0.023	0.018	0.027	0.016	0.018	0.023
Nb	<0.2	<d.l.	<d.l.	<d.l.	<d.l.	<d.l.	<d.l.	<d.l.	<d.l.	<d.l.	<d.l.
Nd	0.16	0.08	0.32	0.29	0.08	0.3	0.18	0.26	0.17	0.17	0.25
Ni	2430	1540	780	1560	1150	570	1400	1150	840	610	1120
Pb (d.l=<5 ppm)	<5	<d.l.	<d.l.	<d.l.	<d.l.	<d.l.	<d.l.	9	<d.l.	<d.l.	<d.l.
Pr	0.03	0.01	0.05	0.04	0.01	0.05	0.03	0.04	0.03	0.03	0.04
Rb (d.l=<1 ppm)	<1	<d.l.	<d.l.	<d.l.	<d.l.	<d.l.	<d.l.	<d.l.	<d.l.	<d.l.	<d.l.
Sb (d.l=<0.2 ppm)	<0.2	3.2	4.1	2.4	2.5	<d.l.	1.6	2.3	0.7	<d.l.	0.9
Sc	8	8	13	9	7	10	8	12	8	8	12
Sm	0.04	0.03	0.14	0.12	0.03	0.11	0.07	0.11	0.06	0.06	0.1
Sr (d.l=<2 ppm)	<2	<d.l.	4	<d.l.	<d.l.	31	18	21	26	15	15
Ta (d.l=<0.01 ppm)	<0.01	<d.l.	<d.l.	<d.l.	<d.l.	<d.l.	<d.l.	<d.l.	<d.l.	<d.l.	<d.l.
Tb	<0.01	<d.l.	0.04	0.04	0.01	0.03	0.02	0.03	0.02	0.01	0.03
Th (d.l=<0.05 ppm)	<0.05	<d.l.	<d.l.	<d.l.	<d.l.	<d.l.	<d.l.	<d.l.	<d.l.	<d.l.	<d.l.
Tl (d.l=<0.05 ppm)	<0.05	<d.l.	0.11	<d.l.	<d.l.	<d.l.	<d.l.	<d.l.	<d.l.	<d.l.	<d.l.
Tm	0.006	0.008	0.037	0.024	0.01	0.021	0.017	0.023	0.013	0.014	0.025
U (d.l=<0.01 ppm)	0.02	<d.l.	<d.l.	<d.l.	<d.l.	<d.l.	0.02	0.1	<d.l.	<d.l.	<d.l.
V	39	19	29	20	14	24	15	26	17	11	29
Y	<0.5	0.6	2.7	1.5	0.6	1.5	0.9	1.6	0.8	0.8	1.5
Yb	0.05	0.06	0.26	0.16	0.08	0.14	0.12	0.16	0.09	0.1	0.16
Zn	<30	40	40	50	50	40	40	60	50	<30	60
Zr (d.l=<4 ppm)	<4	<d.l.	<d.l.	<d.l.	<d.l.	<d.l.	<d.l.	<d.l.	<d.l.	<d.l.	<d.l.

Ludden and Thompson, 1979; Humphris, 1984), fluid speciation, secondary mineralogy and redox conditions (Allen and Seyfried, 2005). Under appropriate conditions, elements that are generally considered immobile, such as Nd, can be transported and thus provide records of fluid–rock interaction (Menzies et al., 1993). In this paper, we compare REE patterns, and Sr and Nd isotope compositions of the basement rocks of the Lost City Hydrothermal Field at the southern ridge of the Atlantis Massif with compositions of the gabbroic and ultramafic rocks drilled at the central dome. These results are used to evaluate the variations in seawater interaction on a regional scale, to quantify water–rock ratios at the southern ridge, and to assess the variations in isotopic compositions of gabbroic rocks at the central dome. We also discuss the influence of fluid–rock interaction on REE mobility in the ultramafic rocks at the Atlantis Massif and the potential of Nd isotopes to better constrain high water–rock ratios (>100) in hydrothermal systems.

2. Methods

2.1. Field sampling

This study is based on field investigations and sampling at the central dome (IODP Site U1309) and at the southern ridge of the Atlantis Massif in the vicinity of the Lost City Hydrothermal Field (Expedition Scientific Party, 2005a,b; Kelley et al., 2005; Blackman et al., 2006) and is part of an extensive geological, petrological and geochemical investigation of the crustal architecture, alteration history and exhumation of the massif as an OCC. The southern ridge of the AM and LCHF were sampled during three cruises: in 2000 and 2003 (cruises AT3-60 and AT7-34) using the submersible *Alvin* with the R/V *Atlantis*; and in 2005 using the remotely operated vehicles (ROV) *Hercules* and *Argus* onboard the R/V *R. H. Brown*. These expeditions collected serpentinites, metagabbros, talc- and amphibole-schists, sediments, basalts, hydrothermal carbonates and fluids (Blackman et al., 2002; Schroeder and John, 2004; Kelley et al., 2005; Boschi et al., 2006; Karson et al., 2006; Ludwig et al., 2006). Preliminary results of the 2005 expedition are available under http://oceanexplorer.noaa.gov/exploration/05lostcity/welcome.html. The geology of the area and studies of the mineral assemblages, bulk rock geochemistry and mass transfer associated with the formation of the detachment shear zone and metasomatic fault rocks are described in detail in Karson et al. (2006) and Boschi et al. (2006).

The geochemical study presented here incorporates petrological, geochemical, and isotopic results produced by our group at the ETH Zurich (e.g., Boschi, 2006; Delacour, 2007; Delacour et al., 2007, 2008). For this study, thirty-one representative samples from the southern wall of the AM were selected for Sr and Nd isotope analyses; their locations are shown in Fig. 1b–c. In addition, twenty samples of representative lithologies were selected at regular depth intervals from the Hole 1309D drillcore (central dome) to monitor downhole variability and one ultramafic sample was selected from the top of Hole 1309B. In addition, the ultramafic lithologies recovered at Hole 1309D (serpentinized harzburgites and olivine-rich troctolites with a poikilitic texture) were sampled in detail for comparison with the serpentinized peridotites of the southern wall.

2.2. Analytical methods

Major element, trace element, and Rare Earth Element (REE) analyses of 11 whole rock samples (Table 1) from the central dome (IODP Holes 1309D and 1309B) were performed at the Activation Laboratories Ltd. (Ancaster, Canada). Major elements were measured with its research high-quality fusion Inductively Coupled Plasma (ICP;

Table 2
Description, location, Sr and Nd isotope compositions, and Sr and carbonate contents of samples from the southern wall

Sample number	Types of rock	Depth	Latitude	Longitude	$CaCO_3$ content	Sr	Nd	$^{87}Sr/^{86}Sr$	$^{143}Nd/^{144}Nd$	ε_{Nd} [b]
		(mbsl)	N	W	wt.%	(ppm)	(ppm)	(±2σ int. error×10^5)	(±2σ int. error×10^5)	(±2σ int. error)
3651-1252	Serpentinite	795	30°7.407′′	42°6.968′	0.07	3.4	0.14	0.708902±13	0.513018±35	7.4±0.69
3863-1301	Serpentinite	834	30°7.512′	42°7.410′	0.06	3.8	0.43	0.709068±10	0.513215±13	11.3±0.26
3863-1526	Serpentinite	778	30°7.476′	42°7.140′	4.18	30.0	0.33	0.709089±10	0.512557±20	−1.6±0.39
3867-1623	Serpentinite	759	30°7.482′	42°7.140′	0.05	3.5	0.43	0.708994±13	0.513202±10	11.0±0.20
3872-1136	Serpentinite	798	30°7.482′	42°7.134′	0.08	3.7	0.56	0.709002±19	0.512887±17	4.9±0.33
3873-1245	Serpentinite	956	30°7.356′	42°7.806′	1.00	22.0	0.08	0.709126±10	0.513064±82	8.3±1.61
3873-1300	Serpentinite	950	30°7.338′	42°7.776′	0.42	3.9	0.06	0.709051±11	0.512742±58	2.0±1.12
3876-1310	Serpentinite	774	30°7.656′	42°7.834′	0.26	5.2	0.07	0.709180±14	0.512397±26	−4.7±0.52
3877-1158	Serpentinite	1115	30°7.026′	42°7.122′	0.11	3.2	0.55	0.709075±17	0.512894±16	5.0±0.32
3877-1307	Serpentinite	1017	30°7.218′	42°7.140′	0.44	50.9	0.59	0.709139±12	0.512926±19	5.6±0.36
3877-1344	Serpentinite	913	30°7.320′	42°7.206′	0.04	2.5	0.08	0.709024±13	0.512997±54	7.0±1.05
3877-1406	Serpentinite	908	30°7.320′	42°7.200′	0.16	4.1	0.26	0.709098±12	0.512576±70	−1.2±1.37
3879-1253	Serpentinite	847	30°7.476′	42°7.170′	1.92	39.0	0.57	0.709012±10	0.512932±18	5.7±0.35
3881-1119	Serpentinite	860	30°7.404′	42°7.128′	0.00	<d.l.	0.21	0.709119±27	0.512903±39	5.2±0.75
3881-1132a	Serpentinite	822	30°7.422′	42°7.098′	0.17	5.5	0.11	0.708932±14	0.513155±44	10.1±0.85
H03-R2243	Serpentinite	834	30°7.246′	42°7.113′	1.05	90.0	0.06	0.708855±13	0.512432±141	−4.0±2.75
H03-R2301	Serpentinite	820	30°7.246′	42°7.109′	0.12	7.0	2.36	0.709027±11	0.513138±16	9.8±0.31
3645-1145	Basalt[a]	957	30°7.355′	42°7.826′	0.50	108.0	11.00	0.703456±16	0.513198±09	10.9±0.17
3863-1236	Chlorite blackwall	837	30°7.512′	42°7.416′	0.05	4.0	0.39	0.705951±16	0.513146±09	9.9±0.19
3863-1419	Talc-rich rock	794	30°7.542′	42°7.356′	0.01	6.0	1.43	0.705648±13	0.513129±23	9.6±0.45
3863-1425	Talc-rich rock	794	30°7.542′	42°7.356′	0.02	5.0	0.79	0.707431±14	0.513199±08	10.9±0.15
3873-1124	Talc-rich rock	959	30°7.416′	42°7.842′	0.33	7.0	0.46	0.707677±13	0.513089±25	8.8±0.49
3873-1344	Talc-rich rock	923	30°7.332′	42°7.686′	0.31	11.0	4.40	0.705337±16	0.512900±07	5.1±0.14
3873-1250	Amphibole schist	956	30°7.338′	42°7.776′	0.00	6.5	2.22	0.704439±16	0.513163±05	10.2±0.10
3877-1313	Amphibole schist	1009	30°7.224′	42°7.140′	0.75	6.9	2.12	0.704837±15	0.513356±38	14.0±0.73
3865-1245	Amphibole schist	795	30°7.452′	42°7.218′	0.01	8.1	7.00	0.704405±16	0.513179±07	10.6±0.13
3867-1254	Gabbro	843	30°7.356′	42°7.200′	0.01	137.0	3.08	0.704294±13	0.513187±05	10.7±0.11
3867-1603	Gabbro	748	30°7.488′	42°7.134′	0.01	139.0	1.84	0.703422±11	0.513178±08	10.5±0.15
3876-1117	Gabbro	869	30°7.458′	42°7.122′	0.01	119.0	3.08	0.703208±12	0.513191±07	10.8±0.14
3876-1215	Gabbro	798	30°7.482′	42°7.140′	0.09	10.0	5.85	0.704619±13	0.513192±07	10.8±0.14
3880-1349	Gabbro	819	30°7.236′	42°7.086′	n.d.	49.6	54.40	0.703630±14	0.513206±06	11.1±0.11

[a] The basalt analyzed is a large clast in sedimentary breccia and is considered to be debris slide material from the hanging wall (Karson et al., 2006).
[b] Epsilon values were calculated with Eq. (1) from the initial $^{143}Nd/^{144}Nd$ relative to CHUR (Nd)=0.512638 (Jacobsen and Wasserburg, 1980). Average bulk rock compositions of the serpentinites from the southern wall are reported in Boschi et al. (2006).

Thermo Jarrell-Ash ENVIRO II or Spectro Cirris) and trace elements were measured by Inductively Coupled Plasma-Mass Spectrometry (ICP-MS; Perkin Elmer SCIEX ELAN 6000 or 6100). Calibration of the ICP and ICP-MS were performed using 11 international standards (SY-3, SY-2, NIST 694, W-2a, DNC-1, BIR-1, GBW 07113, NIST 1633b, STM-1, IF-G, FK-N) and the analytical precision calculated between the measured and certified values of the standards is ±3% for all elements.

The Sr and Nd concentrations of the samples of the southern wall presented in Table 2 were determined by ICP-AES and ICP-MS at the CRPG-Nancy (France) after fusion with $LiBO_2$ and dissolution with HNO_3. Sr and Nd concentrations of the samples of the central dome (IODP Site U1309) presented in Table 3 were determined at the commercial Activation Laboratories Ltd. (see also Table 1) or measured by ICP-AES (JY2000 ULTRACE ICP-AES) during the two IODP expeditions after fusion with $LiBO_2$. The entire set of bulk rock data measured during the two consecutive IODP expeditions are available as supplementary data of Blackman et al. (2006).

Determination of total inorganic carbon contents (TIC), released as CO_2 from carbonate phases, was carried out at the Geological Institute, ETH Zurich, by coulometric titration (Coulometer UIC CM5012). CO_2 was liberated and analyzed by reaction of HCl with 20 to 30 mg of bulk rock powder in glass capsules. Carbonate contents were calculated from measured TIC based on the assumption that only calcium carbonate ($CaCO_3$, either as aragonite or as calcite) is present (Ludwig et al., 2006). Relative precision of carbon content for replicate measurements of varying weights of calcium carbonate standard (99.95% $CaCO_3$) was ±2% (n=17).

Strontium and Nd isotope measurements (Tables 2 and 3) were carried out at the Institute of Isotope Geochemistry and Mineral Resources (IGMR), ETH Zurich. Samples were selected that contained no or minor late-stage carbonate veins. Prior to chemical treatment, 0.5 g of rock powder was rinsed twice in deionized water (Milli-Q system) to remove seawater contribution/contamination and to ensure measurement of the true Sr and Nd isotope compositions of the samples. Before chemical separation, the rock powders were dissolved and digested in a mixture (1:1) of concentrated HNO_3 and concentrated HF under high pressure for about 5–6 days. After high-pressure digestion, the samples were evaporated, transferred and dissolved in concentrated HNO_3 for a day on a hotplate. This process was repeated three times with evaporation on the hotplate between each dissolution step. Before starting the separation and purification procedure with ion-exchange chromatography, the samples were transferred to 6 M HCl and finally dissolved in 1 M HCl. Chemical separation and purification were performed using the procedures described by Cohen et al. (1988) for Nd and Horwitz et al. (1992) for Sr.

Due to the low carbonate contents (in general <0.75 wt.%; Tables 2 and 3), no leaching with acetic acid was performed beforehand to remove the carbonate component from the rock powder. Fig. 2 shows that Sr contents do not correlate with carbonate contents, even for samples that contain up to 4.2 wt.% carbonate. This suggests that the presence of minor carbonate veins in the samples has not resulted in an addition of Sr and does not influence the bulk Sr isotope compositions (see also Boschi et al., 2008). In fact, simple mass balance calculations show that the addition of 4.5 wt.% of carbonate with a Sr concentration of 1500–2000 ppm and $^{87}Sr/^{86}Sr$ ratios of ~0.7086 (Plank and Langmuir, 1998) would not lead to the seawater-like values characteristic of the serpentinites of the southern wall of the AM. In addition, acid leaching to remove the carbonates may alter the phyllosilicate minerals resulting in a loss of Sr from the rock sample.

Sr and Nd isotope ratios were determined using a Nu Instruments Multicollector Inductively Coupled Plasma Mass Spectrometer (MC-ICPMS). For Sr isotope measurements, interference of ^{86}Kr (from the Ar carrier gas) and possible ^{87}Rb contributions on the respective Sr masses was monitored through the simultaneous measurement of ^{83}Kr and ^{85}Rb. Interference-corrected $^{87}Sr/^{86}Sr$ ratios were adjusted for mass bias internally by normalizing to a $^{86}Sr/^{88}Sr$ ratio of 0.1194 (Nier, 1938; Steiger and Jager, 1977). The elevated scattered back-

Table 3
Description, location, Sr and Nd isotope compositions, and Sr and carbonate contents for samples from Hole 1309D (30°10.12′N, 42°7.11′W, 1656.0 mbsl) and Hole 1309B (30°10.11′N, 42°7.11′W, 1653.4 mbsl)

Hole/leg	Sample number	Piece	Types of rock	Depth (mbsf)	Alteration (%)	Sr (ppm)	Nd (ppm)	$CaCO_3$ content wt.%	$^{87}Sr/^{86}Sr$ (±2σ int. error×10^5)	$^{143}Nd/^{144}Nd$ (±2σ int. error×10^5)	ε_{Nd} [a] (±2σ int. error)
304-1309D	1R-1 72–80 cm	3B	Basalt	21.2	50	92	n.d.	0.084	0.702962±11	0.513201±07	11.0±0.14
304-1309D	1R-3 4–8 cm	1	Talc/amph schist	23.3	100	2	4.37	0.106	0.704477±14	0.513161±13	10.2±0.26
304-1309D	17R-2 9–17 cm	1	Olivine gabbro	100.0	40	n.d.	n.d.	0.101	0.702841±14	0.513174±12	10.5±0.25
304-1309D	31R-2 19–30 cm	2	Harzburgite	173.2	90	32	n.d.	4.000	0.709036±11	0.513261±65	12.1±1.27
304-1309D	42R-1 0–8 cm	1	Talc-rich harzburgite	224.3	90	4	0.32	0.686	0.708571±15	0.513381±76	14.5±1.48
304-1309D	51R-4 30–38 cm	1A	Gabbro	271.0	10	86	n.d.	0.196	0.702686±11	0.513185±10	10.7±0.21
304-1309D	60R-3 35–45 cm	4	Troctolite	313.2	50	n.d.	n.d.	0.225	0.703354±12	0.513107±46	9.1±0.89
304-1309D	65R-2 22–30 cm	3B	Cr-rich harzburgite	335.7	50	n.d.	0.08	2.755	0.706870±79	0.513059±71	8.2±1.39
305-1309D	83R-1 16–26 cm	2A	Olivine gabbro	415.2	5	54	n.d.	0.144	0.702721±12	0.513149±17	10.0±0.33
305-1309D	83R-1 53–64 cm	2B	Olivine gabbro	415.5	50	n.d.	n.d.	3.482	0.703202±12	0.513197±14	10.9±0.26
305-1309D	84R-2 8–17 cm	1A	Oxide-/leucogabbro	421.0	60	n.d.	n.d.	4.025	0.703698±12	0.513205±12	11.1±0.23
305-1309D	87R2 63–71 cm	2E	Oxide gabbro	436.3	20	95	n.d.	0.948	0.702857±12	0.513205±07	11.1±0.14
305-1309D	100R-1 42–46 cm	1B	Olivine-rich troctolite	497.0	10	44	n.d.	0.127	0.702688±10	0.513171±22	10.4±0.44
305-1309D	116R-1 58–68 cm	2F	Oxide-/leucogabbro	574.0	50	n.d.	n.d.	2.158	0.703604±13	0.513192±11	10.8±0.22
305-1309D	136R-2 21–29 cm	2A	Olivine gabbro	671.0	20	29	n.d.	0.166	0.702814±12	0.513167±19	10.3±0.37
305-1309D	137R-2 85–91 cm	4	Oxide gabbro	675.1	40	n.d.	n.d.	0.080	0.702709±12	0.513187±09	10.7±0.19
305-1309D	169R-1 90–100 cm	3D	Gabbro	823.9	5	102	n.d.	0.159	0.702627±12	0.513221±10	11.4±0.19
305-1309D	227R-3 6–12 cm	2A	Olivine-rich troctolite	1095.0	50	30	n.d.	0.199	0.702686±13	0.513129±38	9.6±0.73
305-1309D	237R-2 6–18 cm	1B	Olivine-rich troctolite	1140.6	10	21	0.26	0.201	0.702693±10	0.513227±07	11.5±1.35
305-1309D	292R-2 78–88 cm	4	Gabbro	1398.6	20	n.d.	n.d.	0.172	0.702614±12	0.513203±08	11.0±0.16
304-1309B	11R-1 23–31 cm	1B	Harzburgite	58.6	90	2	n.d.	0.348	0.708862±06	n.d.	n.d.

[a] Epsilon values were calculated with Eq. (1) from the initial $^{143}Nd/^{144}Nd$ relative to CHUR (Nd)=0.512638 (Jacobsen and Wasserburg, 1980).

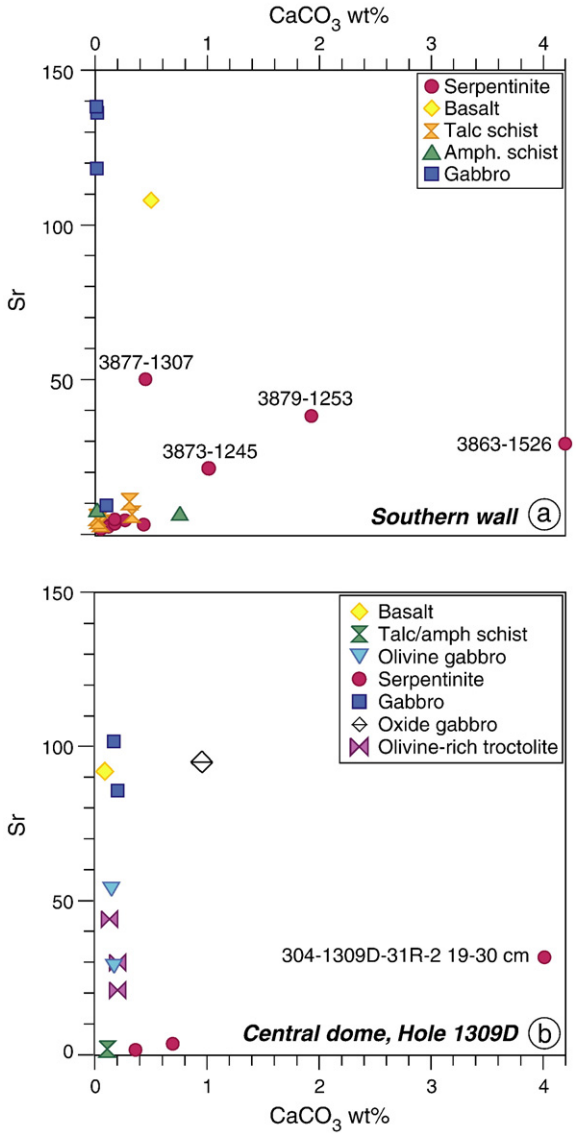

Fig. 2. Sr contents versus total carbonate contents for a. samples from the southern wall of the Atlantis Massif and b. samples recovered from Hole 1309D at the central dome. The lack of correlation between Sr contents and carbonate contents suggests that the presence of minor carbonate does not increase Sr contents in the rocks and therefore has negligible influence on Sr isotope compositions.

ground in the Sr mass range was accounted for by subtracting linearly interpolated zero beam intensities on 1/3 masses above and below the mass of interest. Measured Nd isotope compositions were normalized internally to $^{146}Nd/^{144}Nd = 0.7219$ to correct for instrumental mass bias. For interlab comparison, Sr isotope ratios were normalized to $^{87}Sr/^{86}Sr$ of 0.710245 for NIST SRM987, and Nd isotope ratios were normalized to the JNdi-1 standard $^{143}Nd/^{144}Nd$ of 0.512115 (Tanaka et al., 2000). The external reproducibility for repeated measurements of the NIST SRM987 Sr standard was 0.000025 (2σ; $n=47$) and 0.000015 (2σ, $n=44$) for the JNdi-1 Nd standard. The in-run precision for each sample was better than external reproducibility, except for samples with very low concentration in Nd. The $^{143}Nd/^{144}Nd$ results presented here are expressed in standard epsilon notation relative to a Chondrite Uniform Reservoir (CHUR):

$$\varepsilon_{Nd} = \left[\frac{^{143}Nd/^{144}Nd_{sample}}{^{143}Nd/^{144}Nd_{CHUR}} - 1\right] \times 10^4 \quad (1)$$

with $^{143}Nd/^{144}Nd_{CHUR} = 0.512638$ (Jacobsen and Wasserburg, 1980).

3. Regional-scale heterogeneity of the Atlantis Massif

The Atlantis Massif (30°N) is located 15 km west of the Mid-Atlantic Ridge (MAR) axis, at the inside corner of the intersection between the Atlantis Transform Fault (Fig. 1a) and the MAR, and is a dome-like massif interpreted as an oceanic core complex (OCC) (Cann et al., 1997; Blackman et al., 1998; Collins et al., 2001; Blackman et al., 2002; Karson et al., 2006; Ildefonse et al., 2007). Based on morphologic and lithologic criteria, this 1.5 to 2 Ma old massif is divided into three domains: the peridotite-dominated southern ridge, the gabbroic central dome, and the volcanic eastern block (Fig. 1a). The surface of the central dome is marked by parallel corrugations and striations, which are interpreted as surface expressions of a low-angle detachment fault that led to the uplift and exposure of the massif on the ocean floor (Cann et al., 1997; Blackman et al., 1998, 2002; Karson et al., 2006). The eastern block (Fig. 1a) consists predominantly of basaltic rocks that are interpreted as forming the hanging wall of the OCC (Karson et al., 2006).

The southern ridge of the AM differs from the central dome in rock composition and by the proportion of ultramafic to mafic lithologies. In the south, the top of the massif lies at water depths of 700–800 m and has experienced greater uplift than the central dome (1650 m water depth) ~5 km to the north. Karson et al. (2006) postulated that a major discontinuity occurs between the central dome and the southern ridge. This discontinuity may be a fault zone or represent the limit of a gabbroic intrusion. Normal faulting and mass wasting along the southern part of the AM have resulted in a near-vertical 3800 m-high, transform-parallel scarp that provides a window into the basement below the Lost City Hydrothermal Field (Kelley et al., 2005; Karson et al., 2006).

3.1. Lithologies and alteration history of the southern ridge

Dredging and submersible sampling of the scarp that forms the southern wall recovered predominantly serpentinized peridotites (~70%) with interspersed minor gabbroic bodies (~30%) (Blackman et al., 2002; Schroeder and John, 2004; Boschi et al., 2006; Karson et al., 2006). The peridotites are primarily depleted spinel harzburgites, consisting of olivine, orthopyroxene and chromium spinel. The primary olivine and orthopyroxene are affected by a high degree of serpentinization (from 70 to 100%) and are replaced by serpentine, magnetite and minor chlorite, amphibole and talc. Multiple phases of serpentine growth and overprinting textures suggest that seawater penetration and serpentinization commenced close to the ridge axis and continued throughout the tectonic evolution of the massif. Oxygen isotope compositions are generally depleted in ^{18}O (+1.7 to +5.5‰ V-SMOW) and indicate that alteration was most pervasive at temperatures of approximately 150–250 °C (Boschi et al., 2008). The predominance of magnetite associated with very low amounts of pyrite in the serpentinites reflect slightly oxidizing conditions during serpentinization (Delacour et al., 2005, 2007). In addition, Fe–Ni alloys and brucite, which are minor phases sensitive to oxygen fugacity, were not identified in the serpentinites at the southern wall.

The gabbroic rocks at the southern AM include variably altered and deformed medium- to coarse-grained gabbro, oxide gabbro, gabbro-norite, pyroxenite, and microgabbro. Primary minerals consist of plagioclase, clinopyroxene, oxide phases, and minor amounts of orthopyroxene. Alteration mineral assemblages record deformation and recrystallization from high-grade granulite to greenschist facies metamorphism and local rodingitization (Schroeder and John, 2004; Boschi et al., 2006; Karson et al., 2006). Overprinting under greenschist facies conditions is characterized by the presence of actinolite and tremolite, and a local late phase of alteration is marked by the presence of zeolite and prehnite veins that cut the higher temperature mineral assemblages and deformation fabrics. The gabbroic rocks contain igneous sulfur mineral assemblages (pyrrhotite+

chalcopyrite+pentlandite) associated with minor secondary pyrite and magnetite (Delacour et al., 2005, 2007).

Less deformed mafic and ultramafic rocks comprising the basement grade into an ~100 m-thick detachment shear zone (DSZ), which consists of highly deformed serpentinites and metagabbros that can be traced continuously for at least 3 km in the tectonic transport direction (Boschi et al., 2006; Karson et al., 2006). This zone is marked by talc and/or amphibole metasomatism related to strain localization and focused fluid flow during exhumation (Schroeder and John, 2004; Boschi et al., 2006). Petrographic and geochemical data indicate that the protoliths of the talc-rich rocks are serpentinized peridotites, whereas amphibole-rich metasomatic rocks are dominated by protoliths of mafic composition (Boschi et al., 2006). Pelagic chalk, limestones and sedimentary breccias with basaltic and serpentinized peridotite clasts cover the mylonitic DSZ (Früh-Green et al., 2003; Kelley et al., 2005; Karson et al., 2006). In the south, this relatively well-lithified carbonate cap sequence is believed to act as a barrier for heat and hydrothermal fluids produced by the LCHF (Früh-Green et al., 2003; Kelley et al., 2005).

The LCHF is located on a fault-bounded terrace of the southern wall and is composed of numerous active and inactive carbonate-brucite chimneys (Kelley et al., 2001; Früh-Green et al., 2003; Kelley et al., 2005; Ludwig et al., 2006). The hydrothermal chimneys are made of variable proportions of aragonite, calcite and brucite formed by mixing of low-temperature (<90 °C), high-pH (9 to 11) hydrothermal fluids with ambient seawater (Ludwig et al., 2006). The vent fluids are poor in metals, silica and CO_2, but have elevated hydrogen, methane and calcium concentrations derived from serpentinization and provide ideal conditions for thermophilic methane- and sulfur-cycling microbial communities within the hydrothermal structures and subsurface (Schrenk et al., 2004; Kelley et al., 2005; Brazelton et al., 2006; Proskurowski et al., 2006). Lithospheric cooling and subsurface exothermic mineral–fluid reactions in the underlying mantle rocks have driven hydrothermal activity at this site for at least 30,000 years (Früh-Green et al., 2003), and recent U–Th analyses indicate that this is a minimum age (Ludwig et al., 2005, 2006).

The southern wall is cut by a series of NW-trending faults (Fig. 1b) that are roughly parallel to the nearby Atlantis Transform Fault and are interpreted as major steeply dipping faults that control much of the focused flow throughout the field (Kelley et al., 2005; Karson et al., 2006). In addition, sub-horizontal foliations in the basement rocks provide permeable pathways for nearly horizontal sheet-like fluid flow, which locally produces hydrothermal mineral growths that reach up to 10 m in height (Kelley et al., 2005; Ludwig et al., 2006). Transform-parallel faults with significant vertical offsets are typical of many other oceanic massifs that have formed near ridge-transform intersections and may be important features to promote long-lived serpentinization in such massifs (Lagabrielle et al., 1998; Karson, 1998).

3.2. Crustal architecture and alteration at the central dome: IODP Site U1309

The central dome of the AM was the target of Expeditions 304 and 305 of the Integrated Ocean Drilling Program (IODP) in 2004–2005 and two main holes (Hole 1309B and Hole 1309D) were drilled (Fig. 1a) at depths between 1653 and 1885 m below sealevel (mbsl) (Expedition Scientific Party, 2005a,b; Blackman et al., 2006). Five shallow-penetration holes (Hole 1309A and Holes 1309E-H) were dedicated to recovering the sedimentary rocks and the upper surface of the dome corresponding to the detachment fault (Blackman et al., 2006). The main hole (Hole 1309D) penetrated to 1415.5 m below sea floor (mbsf) and consists predominantly of gabbroic rocks (91.4% of the total recovery) with intercalated minor ultramafic rocks (harzburgites and olivine-rich troctolites). The gabbroic rocks at Hole 1309D are compositionally diverse and comprise gabbro (55.7% including gabbronorite), olivine gabbro/troctolitic gabbro (25.5%), troctolite (2.7%) and oxide gabbro (7.0%). Tholeiitic basalts and diabases (2.9%) are more common in the upper part of Hole 1309D but occur locally throughout the hole where they intrude other lithologies.

Preliminary shipboard results indicate that the gabbros at Site U1309 are amongst the most primitive rocks collected along the MAR (Expedition Scientific Party, 2005a,b; Blackman et al., 2006). Primary minerals in the gabbroic rocks are plagioclase and clinopyroxene, with minor amounts of olivine, orthopyroxene and oxides, in variable proportions. The oxide gabbros are composed of plagioclase, clinopyroxene, >2% Fe–Ti oxides, and accessory phases (apatite, zircon and titanite). Leucogabbros are often associated with oxide gabbros and are

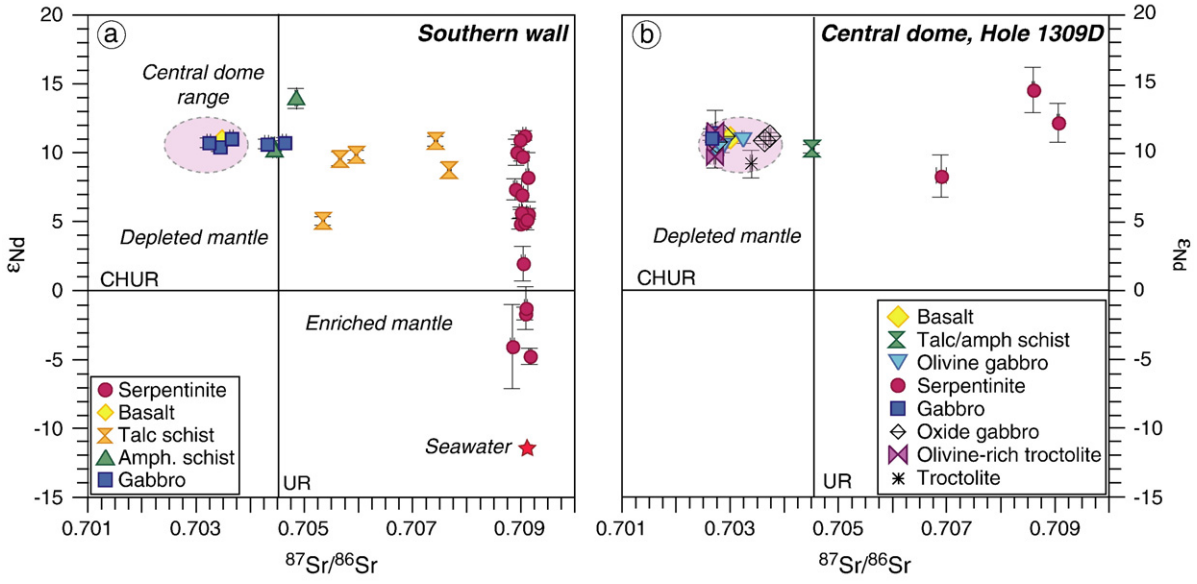

Fig. 3. Variation in ε_{Nd} versus $^{87}Sr/^{86}Sr$ for samples a. from the southern wall of the Atlantis Massif and b. drilled at IODP Hole 1309D of the central dome. The internal error-bars (2σ), the ε_{Nd} composition of the CHUR (CHondritic Uniform Reservoir of 0.512638), and the Sr isotope composition of the UR (Uniform Reservoir of 0.7045) are shown for reference. See text for discussion.

common below 140 mbsf (Expedition Scientific Party, 2005a,b; Blackman et al., 2006). They consist of albite and minor chlorite after plagioclase, and pyroxenes are replaced by green-brown and brown amphiboles. Accessory phases include titanite, epidote, apatite, zircon and calcite (Expedition Scientific Party, 2005a,b; Blackman et al., 2006).

Alteration mineral assemblages in the gabbroic rocks record cooling and local fluid–rock interaction from magmatic conditions to zeolite facies, with a predominance of moderate temperature alteration (<500 °C). The degree of alteration in the gabbroic rocks decreases downhole (Expedition Scientific Party, 2005a,b; Blackman et al., 2006): alteration is moderate in the upper 400 m (average ~ 50%), low between 400 and 800 mbsf (average ~ 30%) and minor between 800 and 1415 mbsf (average ~ 10%). Recrystallization during granulite–amphibolite facies metamorphism was limited and greenschist facies assemblages are characterized by secondary plagioclase and chlorite after igneous plagioclase, and tremolite and actinolite as rims around primary pyroxene. In olivine-bearing rocks, plagioclase is altered to a hydrous mineral assemblage of prehnite, hydrogarnet and chlorite, and olivine is altered to serpentine and magnetite forming ribbon to mesh texture and/or rimmed by tremolite and minor talc at contacts with plagioclase. The latest zeolite facies phase of alteration is recorded by replacement of plagioclase and the occurrence of zeolite-bearing veins in samples below 800 mbsf (Expedition Scientific Party, 2005a,b; Blackman et al., 2006).

Ultramafic rocks s.l. make up only 5.7% of the total recovered rocks at the central dome and mainly occur as olivine-rich troctolites (5.4% of the total recovery at Hole 1309D). Variably serpentinized (from 50 up to 90%) harzburgites are rare (<0.3% of the total recovery) and occur locally in the upper 225 m of Hole 1309D and in the upper 60 m of Hole 1309B (Expedition Scientific Party, 2005a,b; Blackman et al., 2006). Primary olivine and orthopyroxene are replaced by serpentine, magnetite, and minor tremolite, chlorite and talc; some orthopyroxenes show bending characteristic of high temperature crystal-plastic deformation. Alteration is similar to that of the southern wall and is characterized by well-developed ribbon to mesh serpentine textures, which are crosscut by several generations of serpentine, calcite and talc–tremolite–chlorite veins. The olivine-rich troctolites occur primarily between 1095 and 1236 msbf and display a poikilitic texture with olivine and minor Cr-spinel included within plagioclase and clinopyroxene poikiloblasts. Recent petrostructural and geochemical studies of these rocks suggests a complex crystallization history in an open system with impregnation of MORB-type melts (Drouin et al., 2007). Alteration varies from moderate (50–70%) to low (<5%). Alteration mineral assemblages are similar to those in the olivine-bearing gabbros and are cut by chlorite, tremolite and minor calcite veins.

4. Analytical results

4.1. Strontium and Nd isotope compositions

4.1.1. Southern Atlantis Massif

The variations in strontium and neodymium isotope compositions of samples from the southern ridge are shown in Fig. 3a and Table 2 and reflect large variations in seawater fluxes and fluid–rock interaction during the long-lived alteration history of the massif. The serpentinized peridotites display a narrow range of elevated $^{87}Sr/^{86}Sr$ ratios (0.70885 to 0.70918) distinct from the Lost City end-member fluids (0.70651–0.70683; Ludwig et al., 2006) and are characterized by a wide range of ε_{Nd} values from mantle-like to unradiogenic compositions (from +11.3 to −4.7). The Sr isotope compositions of the serpentinites are similar to that of North-Atlantic seawater ($^{87}Sr/^{86}Sr = 0.70916$; Palmer and Edmond, 1989) and in the range of ultramafic rocks recovered from the Atlantic (Bonatti et al., 1970). Three of the serpentinite samples from the southern wall show higher Sr contents (Fig. 4a) that correlate with the occurrence of carbonate veins (Fig. 2a, Table 2). However, sample 3877–1307 has the highest Sr concentration but contains minor carbonate (Table 2). In the majority of the samples, there is no obvious correlation between Sr isotope composition and Sr content (Fig. 4a), which indicates no depletion or enrichment in Sr during serpentinization or during subsequent interaction of seawater with the serpentinized peridotites. Thus, the elevated $^{87}Sr/^{86}Sr$ ratios in these rocks must indicate Sr isotope exchange (Spooner et al., 1977), which provides important constraints on the amount of seawater that has interacted with the system.

The talc-rich and amphibole-rich rocks have Sr isotope compositions intermediate between depleted mantle and seawater compositions ranging from 0.70440 to 0.70768, although most of the samples lie in a narrower range (0.70440 to 0.70595; Fig. 3a). They are characterized by a wide range of low to radiogenic Nd isotope compositions (5.1 to 14.0). In contrast to the serpentinites, the gabbros have low $^{87}Sr/^{86}Sr$ ratios (0.70321 to 0.70462) and homogeneous ε_{Nd} values (10.2 to 11.1), which are close to MORB values (Fig. 3a) and indicate an oceanic affinity (McCulloch et al., 1980). High Sr contents in some gabbros (Fig. 4a) are likely related to Sr substitution in Ca-

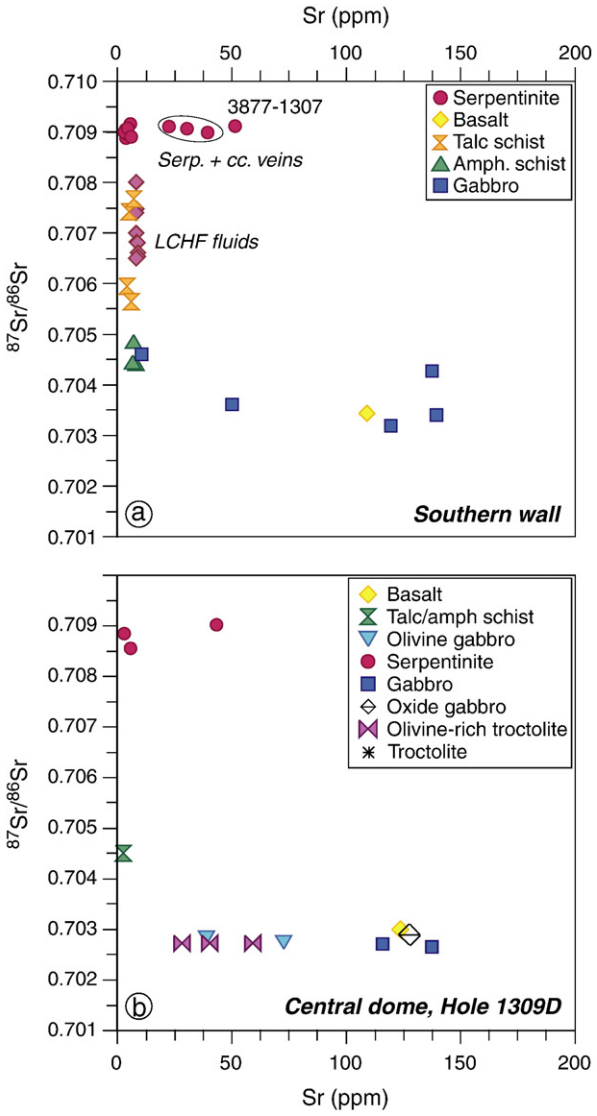

Fig. 4. Variation in $^{87}Sr/^{86}Sr$ ratios versus Sr content for a. the basement rocks from the southern wall of the Atlantis Massif and b. the crustal section drilled at IODP Hole 1309D of the central dome. The lack of correlation between Sr content and $^{87}Sr/^{86}Sr$ ratios indicates no loss or gain of Sr occurred during serpentinization and that Sr isotope exchange is the main process leading to the high $^{87}Sr/^{86}Sr$ ratios.

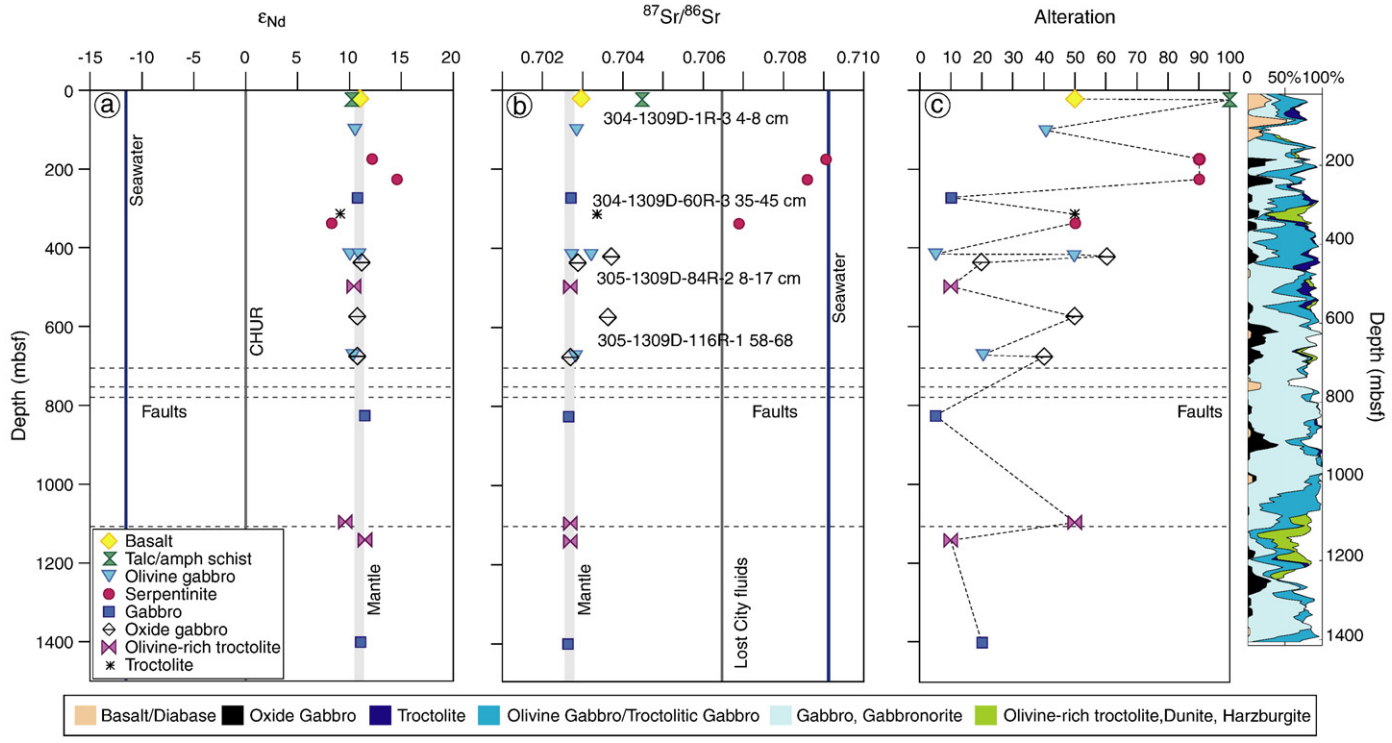

Fig. 5. Comparison of ε_{Nd} values, $^{87}Sr/^{86}Sr$ ratios, and alteration with depth and lithostratigraphy at IODP Hole 1309D at the central dome of the Atlantis Massif. Depths of fault gouges identified by the IODP Shipboard Scientific Party are shown as horizontal dashed lines (695, 756, 785 and 1107 mbsf; Expedition Scientific Party, 2005a,b; Blackman et al., 2006). a. ε_{Nd} values are relatively constant throughout Hole 1309D with minor variations observed in the ultramafic samples (see text for detailed discussion). b. Serpentinized peridotites, basalt and talc-schist concentrated in the upper part of Hole 1309D exhibit high $^{87}Sr/^{86}Sr$ ratios towards seawater composition that correlate with the degree of alteration. Leucogabbros have high $^{87}Sr/^{86}Sr$ ratios, which correlates with the presence of epidote. Sr isotope composition of the Lost City end-member fluid is from Ludwig et al. (2006). c. The crustal section is affected by a moderate to high degrees of alteration in the upper 700–800 mbsf and a low degree of alteration (10–20%) below this depth.

plagioclase and/or substitution in late prehnite replacement and/or veins. The only basalt sample analyzed (a large piece of basalt from a basaltic breccia from the sedimentary cap sequence) yielded $^{87}Sr/^{86}Sr$ and ε_{Nd} values of 0.70346 and 10.9, respectively, similar to those of the gabbros.

4.1.2. Central dome

The samples from Hole 1309D at the central dome show an overall large range of $^{87}Sr/^{86}Sr$ ratios (from 0.70261 to 0.70904; Table 3 and Figs. 3b and 5a–b). In contrast to the southern wall, elevated Sr isotope compositions are restricted to ultramafic lithologies at the top of the hole (Fig. 5a–b) and all samples have Nd isotope compositions (8.2 to 14.5) that lie within a typical oceanic MORB range. The talc/amphibole schist sample (304–1309D-1R-3 4–8 cm) shows a $^{87}Sr/^{86}Sr$ ratio corresponding to the lowest values of talc- and amphibole-rich rocks from the southern wall. In addition, the Hole 1309D gabbroic rocks define a narrow range of Sr and Nd isotope compositions (0.70261–0.70370, average 0.70292; and 9.1 to 11.5, average 10.6, respectively) similar to gabbroic rocks from the southern wall. This indicates that the gabbroic rocks of the Atlantis Massif originated directly from

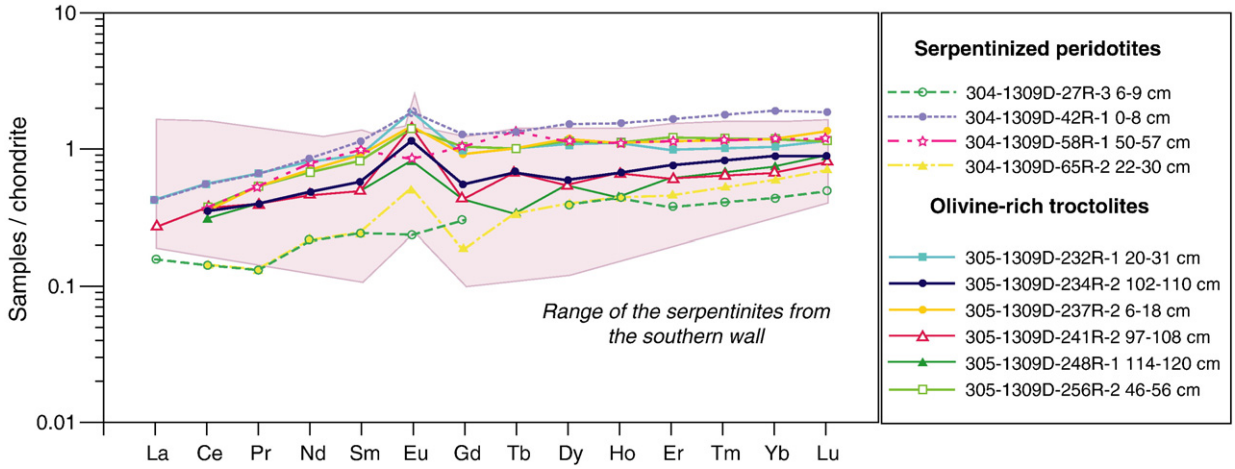

Fig. 6. REE patterns normalized to chondrite (C1; Sun and McDonough, 1989) of the serpentinized peridotites and olivine-rich troctolites of the Atlantis Massif. The serpentinites of the southern wall, represented as shaded area (data from Boschi, 2006), are characterized by enrichment in both LREE and HREE, which is related to hydrothermal alteration and metasomatism and/or entrapment of LREE-rich melts. The serpentinized harzburgites and olivine-rich troctolites from Hole 1309D at the central dome show depletion in LREE and enrichment in HREE characteristic of melt extraction and/or melt-impregnation.

depleted mantle with homogeneous Sr and Nd isotope compositions (Fig. 3).

4.2. Rare earth element compositions

The Rare Earth Element (REE) patterns of the serpentinized peridotites from the southern wall normalized to chondrite (C1; Sun and McDonough, 1989) are characterized by a flat pattern with enrichment in both light REE (LREE) and heavy REE (HREE), which suggests that processes other than progressive equilibrium partial melting have affected the rocks in this region (Fig. 6). Enrichment in LREE is correlated with enrichment in HFSE (e.g., Nb and Y), which can be interpreted as evidence for metasomatism and/or infiltration and entrapment of LREE-enriched melt during crustal accretion (Boschi, 2006). However, as discussed below, these enrichments may also be linked to prolonged seawater–rock interaction and hydrothermal activity during formation of the LCHF.

The REE patterns of the serpentinized harzburgites and olivine-rich troctolites drilled at the central dome (C1; Sun and McDonough, 1989) are depleted in LREE 6 to 10 times the chondrite-normalized values and are enriched in HREE compared to LREE (Fig. 6). These patterns are characteristic of melt extraction (O'Hanley, 1996) and the variable enrichment in REE may be related to different degrees of partial melting and/or to melt-impregnation by addition of clinopyroxene and plagioclase. The serpentinized harzburgites display positive Eu anomalies and likely reflect reducing conditions during serpentinization processes (Allen and Seyfried, 2005). The olivine-rich troctolites from the bottom of Hole 1309D also exhibit positive Eu anomalies, which may be attributed to preferential incorporation of Eu^{2+} in plagioclase (Sverjensky, 1984). There is no systematic difference in REE concentrations between the serpentinized harzburgites from the top of Hole 1309D and the olivine-rich troctolites from deeper in the hole.

5. Discussion

Strontium isotope ratios are important chemical tracers of seawater interaction with the oceanic crust (Dasch et al., 1973; Hart et al., 1974; Hess et al., 1991; Kempton et al., 1991; Hart et al., 1999). In most studies, O and/or Sr isotopes have been used to estimate fluid sources, fluid fluxes, water–rock (W/R) ratios (McCulloch et al., 1980; Kawahata and Scott, 1990; Agrinier et al., 1996; Alt and Bach, 2006; Gao et al., 2006) and the depth of seawater penetration in ophiolite complexes (Spooner et al., 1977; Jacobsen and Wasserburg, 1979; Bickle and Teagle, 1992) and lower crustal gabbroic sequences (Stakes et al., 1991; Hart et al., 1999; Gillis et al., 2005; Alt and Bach, 2006; Gao et al., 2006). Because neodymium is essentially immobile, the Nd isotope composition of the oceanic crust remains unaffected except at very high W/R ratios (Michard et al., 1983; Michard and Albarède, 1986; Snow and Dick, 1995). Thus, the significant shift in Sr and Nd isotope compositions from mantle compositions in the mafic and ultramafic rocks of the Atlantis Massif (Fig. 3) provide important constraints on the degree of seawater–rock interaction, fluid fluxes and the depth of seawater penetration during formation and alteration of this OCC. The regional differences in isotopic signatures also allow important conclusions to be drawn about the influence of long-lived hydrothermal activity at Lost City on element mobility and uptake.

5.1. Downhole Sr and Nd isotope variations at the central dome

The gabbroic series at the central dome show an overall homogeneous isotopic composition, which is close to mantle compositions and in the range of isotopic compositions of other oceanic gabbros recovered at the MARK area ($^{87}Sr/^{86}Sr$: 0.7022–0.7036 and ε_{Nd}: +8 to +13, Leg 153; Kempton and Hunter, 1997), at ODP Site 735B (Hart et al., 1999; Holm, 2002), and at Hess Deep (Gillis et al., 2005). However, some major variations in Sr and Nd isotope compositions away from mantle values are concentrated in the upper 800 mbsf of Hole 1309D (Fig. 5a–b). The talc/amphibole schist sample (304–1309D-1R-3 4–8 cm) shows intermediate Sr isotope compositions between the gabbroic rocks and the serpentinites (Fig. 5b) and the significance of this composition is discussed in Section 5.3. The slightly elevated $^{87}Sr/^{86}Sr$ ratios of mafic samples from the top of Hole 1309D (e.g., 304-1309D-17R-2 9–17 cm located at 100 mbsf; Fig. 5b) are likely related to their stratigraphic position, their higher degree of alteration (Fig. 5c), and the hydrous alteration mineral assemblages; all of which reflect seawater–rock interaction at this depth. Local seawater circulation deeper in the central dome is also indicated by low temperature veins and particularly by the presence of an anhydrite vein within the gabbros at a depth of 739 mbsf (Figure 119A in Blackman et al., 2006). This anhydrite vein, resulting from the precipitation of calcium and sulfate from seawater at temperature >150 °C, is located in fault zones identified between 695 and 785 mbsf (Fig. 5; Expedition Scientific Party, 2005a,b; Blackman et al., 2006) and is associated with zeolite and prehnite, which provide an upper temperature limit of about 250–350 °C. Below these fault zones (>800 mbsf), the isotopic compositions of the gabbros and olivine-rich troctolites are uniform (Fig. 5a–b), which suggests that seawater fluxes and interaction were low and probably limited to (micro)cracks and veins. Similar trends of decreasing $^{87}Sr/^{86}Sr$ ratios and fluid fluxes with depth were reported for the gabbroic rocks of Hole 735B (Kempton et al., 1991; Hart et al., 1999; Bach et al., 2001) and for the extrusive lavas and sheeted dykes of Hole 504B (Teagle et al., 2003; Gillis et al., 2005). In addition, the presence of a fault gouge at 1100 msbf (Expedition Scientific Party, 2005a,b; Blackman et al., 2006) suggests that faults provide pathways for fluid circulation that has likely influenced the isotopic compositions (ε_{Nd} value of +9.6) of one of our olivine-rich troctolite sample (305-1309D-227R-3 6–12 cm). Chemical variations in gabbroic rocks related to the presence of fault zones were also reported by Bach et al. (2001) for the gabbros of Hole 735B.

5.1.1. Seawater–peridotite interaction

The serpentinized peridotites from the top of Hole 1309D and Hole 1309B (304-1309D-31R-2 19–30 cm, 304-1309D-42R-1 0–8 cm, 304-1309D-65R-2 22–30 cm, and 304-1309B-11R-1 23–31 cm) are characterized by the highest $^{87}Sr/^{86}Sr$ ratios (Table 3 and Fig. 5b). These samples are severely altered (50 to 90%; Fig. 5c) and their radiogenic Sr isotope compositions suggest exchange with seawater-derived Sr during serpentinization (Fig. 4a). Their Nd isotope compositions also show some deviations from a typical mantle value to higher ε_{Nd} compositions (Fig. 5a). Similar high ε_{Nd} compositions were measured on peridotites from the Vema Fracture Zone and from the Southwest Indian Ridge (Salters and Dick, 2002; Cipriani et al., 2004), and were interpreted as representing a more depleted mantle component than the mantle source of the MORB (Salters and Dick, 2002; Cipriani et al., 2004). From studies of peridotites dredged from the Vema Fracture Zone, Cipriani et al. (2004) suggested that Nd isotope depletion may have occurred during different events of partial melting.

5.1.2. Water–rock ratios

Water–rock (W/R) ratios, which reflect the extent of seawater–rock interaction in the oceanic lithosphere, were calculated with the Sr and

Table 4
End-members compositions used to model water–rock ratios at the southern wall of the Atlantis Massif

Types of rock	$^{87}Sr/^{86}Sr$	$^{143}Nd/^{144}Nd$	ε_{Nd}[a]	Sr (ppm)	Nd (ppm)
Seawater[b]	0.709160	0.512050	−11.5	8	2.6×10^{-6}
Mantle peridotite[c]	0.702689	0.513181	10.6	6.1	0.483

[a] Epsilon values were calculated with Eq. (1) from the initial $^{143}Nd/^{144}Nd$ relative to CHUR (Nd)=0.512638 (Jacobsen and Wasserburg, 1980).
[b] Sr and Nd isotope compositions are from the literature: Palmer and Edmond (1989) for the Sr isotope compositions and Piepgras and Wasserburg (1987), Tachikawa et al. (1999) for the Nd isotope composition.
[c] Sr and Nd content of mantle peridotites are from Workman and Hart (2005).

Nd isotope compositions of the recovered basement rocks (details are given in the Appendix A). The serpentinized peridotites at the central dome have Sr isotope compositions that correspond to low to moderate W/R ratios (from 2 to 39) and high proportions of Sr isotope exchange (from 63 to 98%; Table 5). These data and the high degree of serpentinization of the peridotite samples (Fig. 5c) provide evidence for circulation of seawater into the oceanic crust. The Sr and Nd isotope compositions of two gabbroic samples located at 313 and 415 mbsf (304-1309D-60R-3 35–45 cm and 305-1309D-83R-1 53–64 cm, respectively) provide constraints on the depth of seawater penetration in the central dome. These two mafic samples show mineral assemblages characteristic of extensive hydration and have both isotopic compositions indicating low W/R ratios of 0.1 (Table 5).

5.1.3. High $^{87}Sr/^{86}Sr$ ratios in leucogabbros

The leucogabbro samples (305-1309D-84R-2 8–17 cm and 305-1309D-116R-1 58–68 cm located at 421 and 574 mbsf, respectively) exhibit relatively high $^{87}Sr/^{86}Sr$ ratios (0.70367 and 0.70360, respectively) compared to the average $^{87}Sr/^{86}Sr$ compositions of the less altered gabbros (0.70281). If we attribute these ratios to seawater–rock interaction, the proportion of Sr isotope exchange with seawater is about 12.5 and 11% for these samples, respectively (Table 5). The origin of the leucogabbros remains equivocal and petrographic analysis does not allow to clearly determine whether they are magmatic leucocratic veins, alteration-products of oxide gabbros or a combination of the two (Expedition Scientific Party, 2005a,b; Blackman et al., 2006). Their elevated Sr isotope compositions may be related to alteration of the primary mineral assemblages to sodic plagioclase and secondary amphibole. Epidote is an important alteration phase in the leucogabbros and may also be significant in controlling the Sr isotope signature of the rocks. Similar elevated Sr isotope compositions are observed in plutonic rocks from the MARK area, and studies of Kempton and Hunter (1997) attribute these to replacement of clinopyroxene by amphibole rather than to plagioclase alteration to albite. From studies of gabbros and sheeted dikes from Hess Deep, Gillis et al. (2005) concluded that albitization of plagioclase results in little or no change in Sr content, whereas epidote formation produces marked Sr enrichment. Similarly, uptake of Sr by epidote during hydrothermal alteration would explain the high $^{87}Sr/^{86}Sr$ ratios of the leucogabbros from Hole 1309D. Further analyses of separate

Table 5
Calculated water–rock ratios for representative samples of the southern wall and central dome

Sample number	Types of rock	Depth	$^{87}Sr/^{86}Sr$	ε_{Nd}[a]	Sr (ppm)	Nd (ppm)	W/R ratios (Sr) Closed system	W/R ratios (Nd)	W/R ratios (Sr) Open system	Sr isotope exchange (%) [b]
Central dome										
304-1309B-11R-1 23–31 cm	Harzburgite	58.55	0.708862	n.d.	2	n.d.	16	n.d.	4.1	95
304-1309D-31R-2 19–30 cm	Harzburgite	173.15	0.709036	12.1	32	n.d.	39	n.d.	5.2	98
304-1309D-42R-1 0–8 cm	Talc-rich harzburgite	224.30	0.708571	14.5	4	n.d.	8	n.d.	3.3	91
304-1309D-60R-3 35–45 cm	Troctolite	313.18	0.703354	9.1	n.d.	n.d.	0.1	n.d.	n.d.	10
304-1309D-65R-2 22–30 cm	Cr-rich harzburgite	335.72	0.706870	8.2	n.d.	0.08	1.4	n.d.	n.d.	65
304-1309D-83R-1 53–64 cm	Olivine gabbro	415.53	0.703202	10.9	n.d.	n.d.	0.1	n.d.	n.d.	8
305-1309D-84R-2 8–17 cm	Oxide-/leucogabbro	420.96	0.703698	11.1	n.d.	n.d.	0.1	n.d.	n.d.	16
305-1309D-116R-1 58–68 cm	Oxide-/leucogabbro	573.98	0.703604	10.8	n.d.	n.d.	0.1	n.d.	n.d.	14
Southern wall and LCHF massif										
3651-1252	Serpentinite	795	0.708902	7.4	3.4	0.14	18	**3.1×10^4**	4.3	96
3863-1301	Serpentinite	834	0.709068	11.3	3.8	0.43	**53**	n.d.	5.6	99
3863-1526	Serpentinite	778	0.709089	−1.6	30.0	0.33	69	**2.3×10^5**	5.9	99
3867-1623	Serpentinite	759	0.708994	11.0	3.5	0.43	**29**	n.d.	4.8	97
3872-1136	Serpentinite	798	0.709002	4.9	3.7	0.56	30	**6.5×10^4**	4.9	97
3873-1245	Serpentinite	956	0.709126	8.3	22.0	0.08	144	**2.1×10^4**	6.9	99
3873-1300	Serpentinite	950	0.709051	2.0	3.9	0.06	44	**1.2×10^5**	5.4	98
3876-1310	Serpentinite	774	0.709180	−4.7	5.2	0.07	n.d.	**4.2×10^5**	n.d.	100
3877-1158	Serpentinite	1115	0.709075	5.0	3.2	0.55	57	**6.3×10^4**	5.7	99
3877-1307	Serpentinite	1017	0.709139	5.6	50.9	0.59	234	**5.4×10^4**	7.5	100
3877-1344	Serpentinite	913	0.709024	7.0	2.5	0.08	36	**3.6×10^4**	5.1	98
3877-1406	Serpentinite	908	0.709098	−1.2	4.1	0.26	79	**2.1×10^5**	6.1	99
3879-1253	Serpentinite	847	0.709012	5.7	39.0	0.57	33	**5.2×10^4**	5.0	98
3881-1119	Serpentinite	860	0.709119	5.2	n.d.	0.21	120	**6.1×10^4**	6.6	99
3881-1132a	Serpentinite	822	0.708932	10.1	5.5	0.11	21	**4.4×10^3**	4.4	96
H03-2243	Serpentinite	834	0.708855	−4.0	90.0	0.06	15	**3.6×10^5**	4.1	n.d.
H03-2301	Serpentinite	820	0.709027	9.8	7.0	2.36	36	**7.3×10^3**	5.1	n.d.
3645-1145	Basalt		0.703456	10.9	108.0	11.00	0.1	n.d.	n.d.	n.d.
3863-1236	Chlorite blackwall	837	0.705951	9.9	4.0	0.39	0.8	n.d.	n.d.	50
3863-1419	Talc-rich rock	794	0.705648	9.6	6.0	1.43	0.6	n.d.	n.d.	46
3863-1425	Talc-rich rock	794	0.707431	10.9	5.0	0.79	2.1	n.d.	2.0	73
3873-1124	Talc-rich rock	959	0.707677	8.8	7.0	0.46	2.6	n.d.	2.2	77
3873-1344	Talc-rich rock	923	0.705337	5.1	11.0	4.40	0.5	n.d.	n.d.	41
3877-1313	Amphibole schist	1009	0.704837	14.0	6.9	2.12	0.4	n.d.	n.d.	33
3865-1245	Amphibole schist	795	0.704405	10.6	8.1	6.98	0.3	n.d.	n.d.	27
3867-1254	Gabbro	843	0.704294	10.7	137.0	3.08	0.3	n.d.	n.d.	25
3867-1603	Gabbro	748	0.703422	10.5	139.0	1.84	0.1	n.d.	n.d.	11
3873-1250	Gabbro	956	0.704439	10.2	6.5	2.22	0.3	n.d.	n.d.	27
3876-1117	Gabbro	869	0.703208	10.8	119.0	3.08	0.1	n.d.	n.d.	8
3876-1215	Gabbro	798	0.704619	10.8	10.0	5.85	0.3	n.d.	n.d.	30
3880-1349	Gabbro	819	0.703630	11.1	49.6	54.40	0.1	n.d.	n.d.	15

The water–rock ratios in bold are in agreement with the modeling curve in Fig. 7.

[a] Epsilon values were calculated from the initial $^{143}Nd/^{144}Nd$ relative to CHUR (Nd) = 0.512638 (Jacobsen and Wasserburg, 1980).

[b] Sr isotope exchange = 100 * ($\varepsilon Sr_{altered\ rock} - \varepsilon Sr_{initial\ rock}$)/($\varepsilon Sr_{seawater} - \varepsilon Sr_{initial\ rock}$) (Davis et al., 2003).

minerals, plagioclase, clinopyroxene, amphibole and epidote are needed to better constrain the controls of mineral composition on the incorporation of radiogenic Sr from the hydrothermal fluid.

5.2. Seawater–peridotite interaction at the southern Atlantis Massif

5.2.1. Constraints from Sr and Nd isotope compositions

The serpentinites from the southern wall of the Atlantis Massif are more than 70% altered and show pronounced changes in Sr and Nd isotope compositions away from mantle compositions (from 0.70885 to 0.70918 and from −4.7 to +11.3, respectively) (Fig. 3a). These isotopic compositions suggest variable degrees of seawater–peridotite interaction during the alteration history of the massif and allow estimations of the fluid fluxes and water–rock ratios in the serpentinites.

Based on the assumptions and equations given in the Appendix A and the compositions of the mantle and seawater end-members presented in Table 4, water–rock (W/R) ratios for closed and open system were calculated for the serpentinized peridotites of the southern part of the AM and are presented in Table 5. A modeling curve calculated for increasing W/R ratios is shown in Fig. 7 for closed and open system conditions, together with the Sr and Nd isotope data of the various lithologies from the southern Atlantis Massif. The shape of the modeling trend implies that for W/R ratios less than 100, only the Sr isotope composition of the rocks is modified towards a seawater composition. At W/R ratios >100, the Sr isotope composition of the rocks reaches that of seawater and cannot change further, at which point the Nd isotope composition starts to be altered towards a seawater composition. The modeling trend is similar for closed and open systems and the differences reside in the absolute values of the W/R ratios for the corresponding Sr and Nd compositions. For example, a W/R ratio of 10 corresponds to Sr isotope compositions of 0.70870 for a closed system and to 0.70916 for an open system modeled with the same Nd isotope values (Fig. 7).

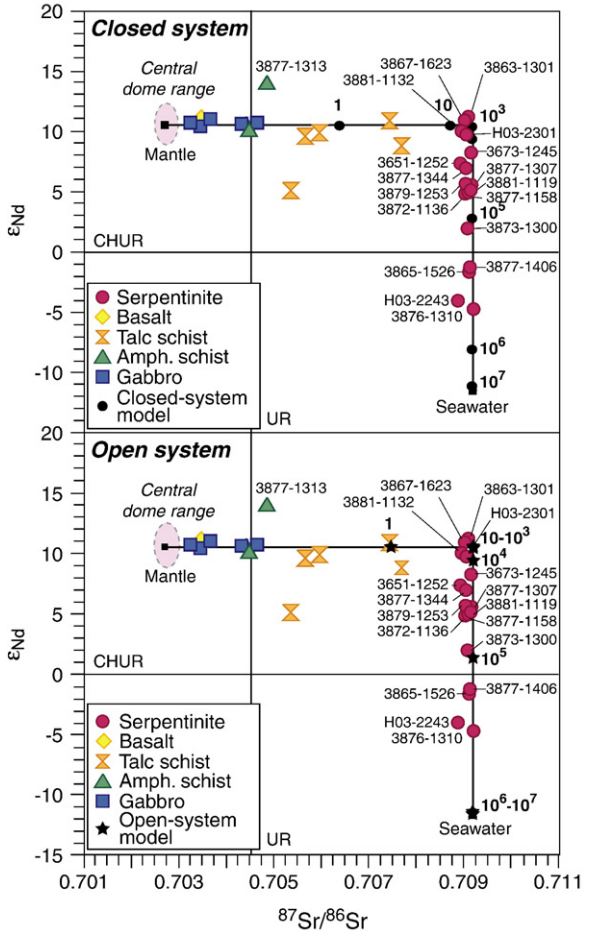

Fig. 7. Relationship of ε_{Nd} values plotted against $^{87}Sr/^{86}Sr$ ratios of the basement rocks of the southern wall of the Atlantis Massif with modeling curves for (a) closed and (b) open system between mantle and seawater end-members. Chemical compositions used for these calculations are reported in Table 4. The numbers close to the modeling curve indicate water–rock (W/R) ratios. The gabbros, basalt and metasomatic fault rocks show low W/R ratios, whereas the serpentinite samples that lie on the descending part of the curve towards seawater signature indicate high W/R ratios.

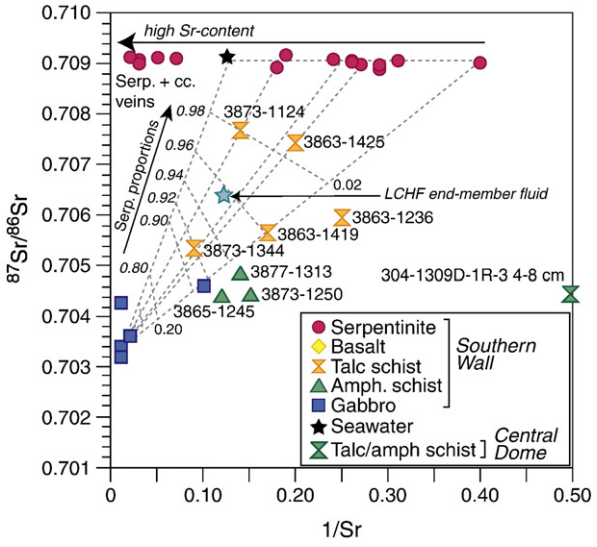

Fig. 8. $^{87}Sr/^{86}Sr$ versus 1/Sr of the basement rocks of the southern wall of the Atlantis Massif. The Sr isotope compositions and Sr contents of the talc-rich samples are related to the mixing of variable proportions of serpentinite and gabbro-derived fluid. Mixing trends are calculated with different Sr contents for the serpentinite end-member and the gabbro-derived fluid end-member is assumed to have similar Sr isotope composition and Sr content as the altered gabbroic rocks. Numbers on the side of the mixing lines indicate the proportions of serpentinite and thus constrain the proportions of gabbro-derived fluids involved in the mixing. The amphibole-rich samples do not lie on the mixing trend, which suggests that they are influenced by other processes, e.g. primary feature of a more depleted mantle or secondary mineral formation during metasomatism.

The serpentinite samples of the southern Atlantis Massif fit the modeling trend very well, especially the part of the curve that approaches seawater end-member compositions (Fig. 7). The Nd isotope compositions of the serpentinites are shifted towards seawater isotopic compositions and indicate very high W/R ratios. Although Nd is considered to be immobile during hydrothermal alteration and metamorphism (Michard et al., 1983; Michard and Albarède, 1986; Négrel et al., 2000), our data clearly show that Nd from seawater has exchanged with Nd in the serpentinized peridotites. Our calculations for a closed system model indicate that the Nd isotope compositions of the serpentinites reflect W/R ratios up to 4.2×10^5 (Table 5).

The gabbros at the southern wall are also affected by seawater interaction as indicated by the hydrous alteration assemblages and depleted O isotope compositions of <5‰ SMOW (Boschi et al., 2008). As shown in Fig. 7, they exhibit somewhat higher $^{87}Sr/^{86}Sr$ ratios than the gabbroic rocks from the central dome (mean value: 0.70292), which corresponds to W/R ratios ranging from 0.1 to 0.3. Similarly, the basalt sample shows the same degree of water–rock interaction as the gabbros with a W/R ratio of 0.1 (Table 5). The higher fluid–rock ratios at the southern Atlantis Massif most likely reflect greater time-integrated fluid fluxes related to the formation of the Lost City hydrothermal system.

5.2.2. Serpentinization and Sr isotope compositions of the LCHF fluids

Strontium isotope compositions of the hydrothermal fluids of the LCHF range between 0.70651 and 0.70683 and are intermediate between the compositions of the mantle peridotites and that of seawater (Figs. 4a and 8; Früh-Green et al., 2003; Ludwig et al., 2006). Their $^{87}Sr/$

^{86}Sr ratios correspond to a mixing between the Sr leached from the underlying mantle peridotites and gabbros and Sr from surrounding seawater (Ludwig et al., 2006). Extrapolation of the $^{87}Sr/^{86}Sr$ ratios of the vent fluids to zero-Mg value gives Sr isotope composition for the LCHF end-member fluid of 0.70640 and a Sr content of 8.3 ppm (Ludwig et al., 2006). This value is lower than the $^{87}Sr/^{86}Sr$ ratios of the LCHF serpentinites but higher than unaltered mantle values and may reflect fluids that have interacted with variably altered mantle peridotites and gabbroic intrusions at depth in the massif. In addition, sampling by submersible does not allow direct sampling of the present-day source region for the hydrothermal fluids, and thus our samples likely represent the most altered "skin" of the active hydrothermal field.

The Sr isotope compositions of the LCHF serpentinites represent an integrated record of seawater–peridotite interaction over the ~1.5 Ma history of the Atlantis Massif. The distinct differences in degree of alteration and in isotopic compositions between the hydrothermal fluids, the basement rocks at the southern wall, and the gabbro-dominated crustal rocks at the central dome clearly reflect differences in seawater fluxes and circulation pathways during the evolution of the massif. Our data together with geological mapping and field observations strongly suggests that transform-parallel as well as transform-orthogonal normal faulting in the south is instrumental in enhancing seawater penetration to sustain hydrothermal activity at Lost City (Fig. 1b; Kelley et al., 2005; Karson et al., 2006).

5.2.3. Comparison of water–rock ratios with other isotopic systems

Isotopic exchange is controlled by mass balance and estimates of water–rock ratios obtained with different isotopic systems will vary depending on the dominant mechanism of exchange during alteration (Hart et al., 1999). For example, strontium isotope exchange is dependant on the mineral–fluid interaction and by formation of secondary minerals, whereas oxygen isotope exchange is temperature-dependant and commonly limited by equilibrium exchange processes with a fluid. Boron isotope exchange is pH-dependant and is strongly controlled by the relative partitioning between trigonal and tetrahedral species (Kakihana et al., 1977; Palmer and Swihart, 1996). These differences are exemplified when we compare water–rock ratios of the serpentinites estimated from Sr and Nd isotopes with estimates obtained from calculations based on O and B isotope compositions (Boschi et al., 2008).

Assuming a closed system model, W/R ratios obtained with stable isotope data are consistently lower than those obtained with Sr and Nd isotope compositions and reflect the limited exchange potential once isotopic equilibrium is reached. Stable isotope data were used to estimate the W/R ratios of the Lost City serpentinites and give W/R ratios of 3 to 7 using O isotope data and approximately 100 with B isotope compositions (Boschi et al., 2008). These W/R ratios are orders of magnitude lower than the W/R ratios estimated from Sr and Nd isotope compositions (21–53 and 4.3×10^3–4.2×10^5, respectively; Table 5). An important result of our companion B and O isotope studies (Boschi et al., 2008) is that B content and $\delta^{11}B$ of the serpentinites at the southern AM are positively correlated, but there is no direct correlation between B content and O isotope composition. These results, together with the distinct lack of late Mg-rich clay minerals, lead to the conclusion that low temperature marine weathering processes are insignificant for mass transfer at the Atlantis Massif. Water–rock ratios calculated with Sr isotopes decrease to a range of 2 to 4 when modeled as an open system (Albarède, 1995) and are in the same order of magnitude as those estimated with O isotopes for a closed system. Our data clearly show that Nd isotopes are most sensitive to high fluid fluxes and are thus an important geochemical tracer for quantification of water–rock ratios in long-lived hydrothermal systems.

5.3. Metasomatic fault rocks: channeled fluids in a heterogeneous lithosphere

The metasomatic fault rocks (talc- and amphibole-rich schists) of the AM (central dome and southern ridge) show intermediate $^{87}Sr/^{86}Sr$ ratios and somewhat scattered but overall mantle-like ε_{Nd} values (Figs. 3a–b, 5a–b and 7). According to our model calculations of water–rock ratios, their isotopic compositions reflect low W/R ratios from 0.3 to 2.6 (Table 5). The amphibole-schist samples yield low W/R around 0.3 and are comparable to those calculated for the gabbros, whereas the talc-rich samples exhibit somewhat higher and variable W/R ratios (Figs. 3a–b and 7, Table 4). On the basis of systematic changes in bulk rock geochemistry, mineralogy and textures, Boschi et al. (2006) argue that the talc-rich fault rocks originate from ultramafic protoliths and formed by the interaction of peridotite with gabbro-derived, oxidizing fluids, rich in Si, Al and Ca, during detachment faulting. They also demonstrate that the bulk rock data of the amphibole-rich rocks point to a mafic protolith (Boschi et al., 2006).

Our results substantiate the conclusions of Boschi et al. (2006). Mixing calculations shown in Fig. 8 indicate that the Sr isotope compositions and concentrations of talc-rich rocks are related to the mixing of two end-members: (i) serpentinite and (ii) a gabbro-derived fluid. The talc-rich rocks exhibit diverse Sr isotope compositions and Sr contents suggesting a variable degree of mixing between the two end-members. In this model, we assume that the gabbro-derived fluid was in chemical and isotopic equilibrium with altered gabbroic rocks, and therefore shows similar $^{87}Sr/^{86}Sr$ ratio and Sr content. Mixing of variable proportions of gabbro-derived fluids with serpentinites, characterized by seawater-like $^{87}Sr/^{86}Sr$ ratios and different Sr contents, lead to compositions similar to those measured in the talc-rich rocks (Fig. 8). For instance, Sr isotope compositions and Sr contents of sample 3873–1124 correspond to 2% of gabbro-derived fluid mixed with a serpentinite protolith with $^{87}Sr/^{86}Sr$ ratios of 0.70905 and a Sr content of ~5–6 ppm (1/Sr of 0.18–0.19).

The amphibole-rich rocks plot off of the mixing trend defined for the talc-rich rocks, indicating that other processes (or starting compositions) are responsible for their high Sr isotope compositions compared to their gabbroic protolith. Formation of secondary amphibole during metasomatism most likely involved seawater-derived fluids and may have thus led to the observed $^{87}Sr/^{86}Sr$ ratios. High Sr isotope compositions of the MARK gabbros have also been attributed to the replacement of clinopyroxene by amphibole (Kempton and Hunter, 1997). Moreover, the amphibole-rich schist 3877–1313 is characterized by the highest radiogenic ε_{Nd} value of 14.0. Boschi et al. (2006) identified the protolith of this amphibole-rich schist as possibly ultramafic due to the presence of Cr-spinel. The high ε_{Nd} value of this sample may thus be a primary feature of a more depleted mantle, as suggested previously for the high ε_{Nd} compositions of the serpentinites of the upper part of Hole 1309D, rather than related to secondary processes of alteration.

The Sr and Nd isotope compositions of the metasomatic fault rocks are similar for the central dome and the southern wall of the Atlantis Massif (Figs. 3, 7 and 8). This suggests that the metasomatic event related to the detachment shear zone (Karson et al., 2006) affected similarly the central dome and the southern part of the AM. This metasomatic event post-dated an early phase of serpentinization close to the ridge axis and was restricted to formation of the detachment fault prior to initiation of Lost City hydrothermal activity (Boschi et al., 2006).

5.4. High fluid fluxes and element mobility

5.4.1. REE patterns as indicators of metasomatism and high water–rock ratios

REEs are generally considered to be immobile elements and not affected by secondary processes and, therefore, can be useful as petrogenetic indicators of primary compositions. However, many studies have demonstrated the mobility of REEs during both aerial and submarine weathering and alteration processes (e.g., Ludden and Thompson, 1979; Nesbitt, 1979; Humphris, 1984; Grauch, 1989; Poitrasson et al., 1995; Négrel et al., 2000). Mobilization of REEs during

fluid–rock interaction depends on three main factors: (1) REE contents of the primary minerals and mineral stability during alteration; (2) REE concentration and speciation in the fluid; and (3) formation of secondary minerals and their affinity for REE (Humphris, 1984).

Menzies et al. (1993) and O'Hanley (1996) argue that REE patterns of serpentinites should be similar to those of the original peridotite protolith, because clinopyroxene, which is the dominant reservoir of REEs, is only slightly altered during serpentinization. However, Leblanc and Lbouabi (1988) suggested that complete serpentinization can fully alter REE patterns, especially if clinopyroxene is a minor phase. This is consistent with experimental studies on seawater–peridotite interaction, which demonstrate that serpentinites formed from harzburgites are characterized by LREE-enrichment (Menzies et al., 1993) and the produced hydrothermal fluids are enriched in LREEs and show positive Eu anomalies (Allen and Seyfried, 2005).

The serpentinized peridotites at the southern wall are characterized by enrichment in both LREEs and HREEs, whereas those of the central dome are LREE-depleted and HREE-enriched (Fig. 6). Although enrichment in LREE may be attributed to early entrapment of LREE-rich melts (Boschi, 2006), comparison of the REE patterns of serpentinites from the two areas of the AM, together with the constraints from Sr and Nd isotope data, suggests that post-magmatic REE mobility may also have occurred during serpentinization and metasomatism at the southern wall. Enrichment in LREE may be related to seawater–rock interaction and the formation of secondary phases, such as serpentine and talc, whereas chlorite preferentially incorporates HREE.

Some samples show slight to pronounced negative or positive Eu anomalies (Fig. 6). The presence of Eu anomalies is commonly related to the presence of plagioclase; however, plagioclase is not present as mineral phase in the serpentinites of the southern wall, which implies another process is responsible for the Eu anomalies. Speciation of REE (e.g., Eu) is influenced by many factors, such as redox conditions, temperature, pressure, dissolved H_2 and dissolved chloride or other complexing agents (e.g., SO_4^{2-}, F^- or HCO_3^-; Sverjensky, 1984; Douville et al., 2002; Allen and Seyfried, 2005). High dissolved chloride concentrations, low pH, high temperature and highly reducing conditions during serpentinization increase REE solubility and therefore lead to Eu anomalies (e.g., at the Rainbow hydrothermal field; Douville et al., 2002; Allen and Seyfried, 2005). While the conditions of serpentinization at the southern AM are slightly oxidizing conditions and relatively low temperature (Delacour et al., 2005; Früh-Green et al., 2005; Delacour et al., 2007), high W/R and seawater-like Cl concentrations of the altering fluids may have favored Eu in a divalent state (Kelley et al., 2001; Allen and Seyfried, 2005).

5.4.2. Importance of Nd isotopes in water–rock ratio models for hydrothermal systems

Estimates of seawater–rock interaction and water–rock ratios using Sr isotope ratios of samples from previous studies of the Troodos ophiolite (Spooner et al., 1977; Bickle and Teagle, 1992), the Cretaceous Samail ophiolite (McCulloch et al., 1980), or the Bay Islands Ophiolite Complex (Jacobsen and Wasserburg, 1979) generally yield values of less than 100. Nd isotope compositions were determined in some of these studies; however, since W/R ratio >100 necessary for complete obliteration of the original igneous Sr isotope composition was not reached, their Nd isotope compositions were not affected by seawater interaction. Snow and Dick (1995) reported similar high Nd isotope compositions for abyssal peridotite samples and argued that these values were related to marine weathering rather than serpentinization. Marine weathering is evidenced by several geochemical criteria (e.g., loss of Mg, presence of clays, high Rb content, Ce anomalies) that are not observed in the serpentinites of the southern wall. In addition, B and O isotope studies indicate that marine weathering is not significant at the southern wall (Boschi et al., 2008). Therefore, we conclude that the high Nd isotope compositions are a consequence of high fluid fluxes. Our studies, thus, document the effect of seawater circulation on the Nd isotope compositions of oceanic basement rocks and the importance of Nd isotopes to estimate water–rock ratios, especially in serpentinites, in an active hydrothermal system. Seawater fluxes into the basement, fluid–rock interaction, and hydrothermal circulation and venting at Lost City are likely enhanced by volume expansion during serpentinization and steep normal faults and mass wasting associated with uplift along the Atlantis Transform Fault (Fig. 1a–b).

6. Conclusions

Our study documents for the first time the combined use of Sr and Nd isotope data, as well as REE concentrations, to monitor fluid–rock interaction in oceanic basement rocks related to an active peridotite-hosted hydrothermal system. The study of the southern ridge and central dome of the Atlantis Massif allow us to evaluate the effects of the Lost City hydrothermal system on fluid fluxes, hydrothermal alteration and metasomatism of the basement rocks within an oceanic core complex. The isotopic compositions and REE patterns of the lower crustal section at Site U1309 indicate that the central part of the massif remained essentially unaffected by Lost City hydrothermal activity and circulation. Seawater interaction is concentrated in the upper part of Hole 1309D and is reflected by high Sr isotope compositions related to serpentinization of peridotites, whereas mantle-like isotopic compositions are preserved in the gabbroic rocks and attest to limited seawater interaction at depth. Penetration and interaction of seawater-derived fluids in the gabbroic section was likely limited to crack networks and veins or to the presence of fault zones identified at various depths (e.g., 696–785, 1100 mbsf).

Compared to these background compositions, those of the serpentinites and gabbros of the southern wall reflect significant seawater fluxes and fluid–rock interaction. The isotopic compositions of the gabbroic rocks at the southern wall are slightly higher than those of the central dome and thus indicate a higher degree of seawater alteration and hydrothermal circulation. Moreover, the serpentinites exhibit seawater-like Sr isotope compositions and ε_{Nd} values that range from mantle-like values to unradiogenic compositions and must reflect high time-integrated fluid fluxes related to hydrothermal circulation at Lost City and long-lived serpentinization in the southern part of the Atlantis Massif. Compared to the LREE contents of the serpentinites at the central dome, which are typical of partial melting and depleted abyssal peridotites affected by melt impregnation, the serpentinites at the southern wall show LREE-enrichment that may be related to metasomatism and hydrothermal alteration and/or a higher degree of melt-rock reaction. Although REEs are commonly considered to be immobile and are used as petrogenetic indicators of primary compositions, our study suggests that the high fluid fluxes (>100) may enhance the mobility of REE, particularly that of Nd.

We conclude that the long-lived hydrothermal circulation, serpentinization and metasomatism at the southern wall led to enrichment in some LREE in the serpentinites and the change of mantle-like Nd isotope compositions to unradiogenic seawater-like compositions. Our study shows that Nd isotopes are most sensitive to high fluid fluxes and thus represent important geochemical tracers of water–rock ratios during serpentinization and seawater circulation in such peridotite-hosted hydrothermal systems. An important implication of our results is that high fluxes and long-lived serpentinization processes may be critical to the formation of Lost City-type systems and that transform-related normal faults and mass wasting along the southern wall facilitates seawater penetration necessary to sustain hydrothermal activity.

Acknowledgements

We thank the captains, crews, and technical staffs of *Alvin*, *Argo II*, and *ABE* aboard R/V *Atlantis* during cruises AT3-60 and AT7-34 to the Atlantis Massif in 2000 and 2003 for their outstanding support of this project. We also acknowledge Chiara Boschi, Jeffrey Karson, Donna

Blackman, and the *Atlantis* and IODP co-chiefs and scientific parties for their significant contributions to the data collection and discussions at sea. The authors thank two anonymous reviewers and the associate editor Steven L. Goldstein for their helpful comments which significantly improved our manuscript. The NOAA Ocean Exploration Program to Lost City in 2005 and Bob Ballard provided additional images of key outcrops. This work was supported by Swiss SNF Grants 2100-068055 and 200020-107620 to Früh-Green and NSF Grant OCE-0426109 to Kelley.

Appendix A

The extent of seawater–rock interaction in lithospheric sections is commonly characterized by water–rock (W/R) ratios and can be quantified with Sr and Nd isotope compositions. Water–rock ratios are based on mass balance calculations and assume final isotope equilibrium and were first applied by Taylor (1977) to stable isotope studies and by Spooner et al. (1977) for Sr isotopes. Water–rock interaction in a closed system can be described by the simple mass balance equation:

$$X_w W \varepsilon_w^i + X_r R \varepsilon_r^i = X_w W \varepsilon_w^f + X_r R \varepsilon_r^f \quad (2)$$

In this equation, W is the mass of the hydrothermal fluid, R is the mass of rock being altered by the fluid, ε_r^i is the initial isotopic ratio of the rock, ε_r^f is the final isotopic ratio of the hydrothermally altered rock and is equal to that of the fluid (ε_w^f), ε_w^i is the initial isotopic composition of the hydrothermal fluid (seawater), X_r is the elemental composition of the unaltered rock, and X_w is the elemental composition of the hydrothermal fluid. By rearranging the equation, the water–rock ratio can be calculated as:

$$\left(\frac{W}{R}\right)_{\text{closed-system}} = \left(\frac{\varepsilon_r^i - \varepsilon_r^f}{\varepsilon_r^f - \varepsilon_w^i}\right)\left(\frac{X_r}{X_w}\right) \quad (3)$$

Closed system, or “single-pass”, models assume that all of the unreacted fluid enters the system (i.e. rock) as a single event, equilibrates with the rock and then leaves the system. In contrast, open system, or “multipass”, models are time-integrated models that assume infinitesimally small aliquots of fluid enter the rock, equilibrate and then leave the system before the next aliquot reacts with the rock. Open system water–rock ratios may be obtained by integrating the closed system equation (Albarède, 1995), giving:

$$\left(\frac{W}{R}\right)_{\text{open-system}} = \left(\frac{X_r}{X_w}\right) \ln\left[\left(\frac{\varepsilon_r^i - \varepsilon_r^f}{\varepsilon_r^f - \varepsilon_w^i}\right) + 1\right] \quad (4)$$

Estimates of water–rock ratios are also based on the assumption that the fluid phase (i.e. seawater) and rock are in equilibrium (Albarède et al., 1981) and that Sr and Nd concentrations are not modified during the fluid–rock interaction. The lack of correlation between the Sr isotope compositions and Sr contents of the AM serpentinites (Fig. 4a–b) are consistent with this assumption and indicate that no addition or depletion in Sr occurred during seawater interaction and serpentinization. Thus, we can conclude that the main mechanism leading to the Sr isotope compositions of the serpentinites is Sr isotope exchange (Spooner et al., 1977). Moreover, the calculations are based on dissolution of primary minerals, a process during which Sr is first leached from primary minerals and then precipitated and incorporated into secondary phases without loss to the fluid (Berndt et al., 1988).

The compositions of the mantle and seawater end-members we used to calculate the modeling trend of fluid–rock interaction and the theoretical W/R ratios (Fig. 7) are presented in Table 4. The mantle end-member compositions correspond to the average values of the least-altered olivine-rich troctolites of the central dome for Sr isotope compositions (0.70269) and the average of the gabbroic rocks from the central dome for ε_{Nd} values (0.51318). Literature data were used for Sr and Nd contents of the depleted mantle (Workman and Hart, 2005) and are in agreement with Sr and Nd contents obtained for residual peridotites after 8–18% of partial melting (Boschi, 2006) from a primitive mantle with 19.9 ppm of Sr and 1.25 ppm of Nd (Mc Donough and Sun, 1995). The Sr and Nd contents of seawater are from the literature (Bernat et al., 1972; Brass and Turekian, 1972; Piepgras et al., 1979; Piepgras and Wasserburg, 1980) and the seawater end-member compositions correspond to the present-day values for North-Atlantic seawater ($^{143}Nd/^{144}Nd = 0.51205$; Piepgras and Wasserburg, 1987; Tachikawa et al., 1999; and $^{87}Sr/^{86}Sr = 0.70916$; Palmer and Edmond, 1989) and are consistent with Sr isotope compositions measured for background seawater at the LCHF (Ludwig et al., 2006).

To test for the influence of changes in Sr and Nd composition of seawater during the evolution of the Atlantis Massif over the past 1.5 to 2 million years, we calculated different modeling curves. The Sr isotope evolution was extracted from the seawater curve published by Farrell et al. (1995). Changes of seawater Nd isotope compositions with time were more difficult to assess due to the areal variability of Nd isotope compositions in deep water masses in oceans. The change in Nd isotope composition of deep waters in the North Atlantic over the past 1.5 to 2 Ma was relatively small compared with the differences between the composition of the rocks and seawater (O'Nions et al., 1998; Burton et al., 1999; Reynolds et al., 1999; Abouchami et al., 1999; Frank et al., 2003). Our calculations indicate that the mixing curves do not change significantly with changes in Sr and Nd isotope compositions and thus the evolution of seawater does not substantially influence the estimated water–rock ratios.

References

Abouchami, W., Galer, S.J.G., Koschinsky, A., 1999. Pb and Nd isotopes in NE Atlantic Fe–Mn crusts: proxies for trace metal paleosources and paleocean circulation. Geochim. Cosmochim. Acta 63, 1489–1505.

Agrinier, P., Cornen, G., Beslier, M.-O., 1996. Mineralogical and oxygen isotopic features of serpentinites recovered from the ocean–continent transition in the Iberia Abyssal Plain. Proc. Ocean Drill. Program Sci. Results 149, 541–552.

Albarède, F., 1995. Introduction to Geochemical Modeling. Cambridge Univ. Press. 543 pp.

Albarède, F., Michard, A., Minster, J.F., Michard, G., 1981. $^{87}Sr/^{86}Sr$ ratios in hydrothermal waters and deposits from the East Pacific Rise at 21°N. Earth Planet. Sci. Lett. 55, 229–236.

Allen, D.E., Seyfried, W.E.J., 2005. REE controls in ultramafic-hosted MOR hydrothermal systems: an experimental study at elevated temperature and pressure. Geochim. Cosmochim. Acta 69, 675–683.

Alt, J.C., 1995. Subseafloor processes in mid-ocean ridge hydrothermal systems. In: Humphris, S.E., et al. (Ed.), Seafloor Hydrothermal Systems, Physical, Chemical, and Biological Interactions. Geophys. Monogr. Ser., vol. 91. AGU, Washington, D. C., pp. 85–114.

Alt, J.C., 2003. Hydrothermal fluxes at mid-ocean ridges and on ridge flanks. C. R. Geosci. 335, 853–864.

Alt, J.C., 2004. Alteration of the upper oceanic crust: mineralogy, chemistry and processes. In: Davis, E.E., Elderfield, H. (Eds.), Hydrogeology of the Oceanic Lithosphere. Cambridge Univ. Press, United Kingdom, pp. 495–533.

Alt, J.C., Bach, W., 2006. Oxygen isotope composition of a section of lower oceanic crust, ODP Hole 735B. Geochem. Geophys. Geosyst. 7, G12008. doi:10.1029/2006GC001385.

Bach, W., Alt, J.C., Niu, Y., Humphris, S.E., Erzinger, J., Dick, H.J.B., 2001. The geochemical consequences of late-stage low-grade alteration of lower ocean crust at the SW Indian Ridge: Results from ODP Hole 735B (Leg 176). Geochim. Cosmochim. Acta 65, 3267–3287.

Bach, W., Garrido, C.J., Paulick, H., Harvey, J., Rosner, M., 2004. Seawater–peridotite interactions: first insights from ODP Leg 209, MAR 15°N. Geochem. Geophys. Geosyst. 5, Q09F26. doi:10.1029/2004GC000744.

Bach, W., Paulick, H., Garrido, C.J., Ildefonse, B., Meurer, W.P., Humphris, S.E., 2006. Unraveling the sequence of serpentinization reactions: petrography, mineral chemistry, and petrophysics of serpentinites from MAR 15°N (ODP Leg 209, Site 1274). Geophys. Res. Lett. 33, L13306. doi:10.1029/2006GL025681.

Bernat, M., Church, T.J., Allégre, C., 1972. Barium and strontium concentrations in Pacific and Mediterranean seawater profiles by direct isotope dilution mass spectrometry. Earth Planet. Sci. Lett. 16, 75–80.

Berndt, M.E., Seyfried, W.E.J., Beck, J.W., 1988. Hydrothermal alteration processes at midocean ridges: experimental and theoretical constraints from Ca and Sr exchange reactions and Sr isotopic ratios. J. Geophys. Res. 93, 4573–4583.

Bickle, M.J., Teagle, D.A.H., 1992. Strontium alteration in the Troodos ophiolite: implications for fluid fluxes and geochemical transport in mid-ocean ridge hydrothermal systems. Earth Planet. Sci. Lett. 113, 219–237.

Blackman, D.K., Cann, J.R., Jannsen, B., Smith, D.K., 1998. Origin of extensional core complexes: evidences from the Mid-Atlantic Ridge at Atlantis fracture zone. J. Geophys. Res. 103, 21315–21333.

Blackman, D.K., Karson, J.A., Kelley, D.S., Cann, J.R., Früh-Green, G.L., Gee, J.S., Hurst, S.D., John, B.E., Morgan, J., Nooner, S.L., Kent Ross, D., Schroeder, T.J., Williams, E.A., 2002. Geology of the Atlantis Massif (Mid-Atlantic Ridge, 30°N): implications for the evolution of an ultramafic oceanic core complex. Mar. Geophys. Res. 23, 443–469.

Blackman, D.K., Ildefonse, B., John, B.E., Ohara, Y., Miller, D.J., MacLeod, C.J., the Expedition 304/305 Scientists, 2006. Proceedings Integrated Ocean Drilling Program, 304/305. Integrated Ocean Drilling Program Management International, Inc., College Station TX. doi:10.2204/iodp.proc.304305.2006.

Bonatti, E., Honnorez, J., Ferrara, G., 1970. Equatorial mid-Atlantic ridge: petrologic and Sr isotopic evidence for an alpine-type rock assemblage. Earth Planet. Sci. Lett. 9, 247–256.

Boschi, C., 2006. Building Lost City: Serpentinization, mass transfer, and fluid flow in an oceanic core complex. Ph.D. Thesis No. 16720, ETH Zürich.

Boschi, C., Früh-Green, G.L., Delacour, A., Karson, J.A., Kelley, D.S., 2006. Mass transfer and fluid flow during detachment faulting and development of an oceanic core complex, Atlantis Massif (MAR 30 N). Geochem. Geophys. Geosyst. 7, Q01004. doi:10.1029/2005GC001074.

Boschi, C., Dini, A., Früh-Green, G.L., Kelley, D.S., 2008. Isotopic and element exchange during serpentinization and metasomatism at the Atlantis Massif: insights from B and Sr isotopes. Geochim. Cosmochim. Acta 72, 1801–1823. doi:10.1016/j.gca.2008.01.013.

Brass, G.W., Turekian, K.K., 1972. Strontium distributions in seawater profiles from the Geosecs 1 (Pacific) and Geosecs 11 (Atlantic) test stations. Earth Planet. Sci. Lett. 16, 117–121.

Brazelton, W.J., Schrenk, M.O., Kelley, D.S., Baross, J.A., 2006. Methane- and sulfur-metabolizing microbial communities dominate the Lost City Hydrothermal Field ecosystem. Appl. Environ. Microbiol. 72, 6257–6270.

Burton, K.W., Lee, D.R., Christensen, J.N., Halliday, A.N., Hein, J.R., 1999. Actual timing of neodymium isotopic variations recorded by Fe–Mn crusts in the western North Atlantic. Earth Planet. Sci. Lett. 171, 149–156.

Cann, J.R., Blackman, D.K., Smith, D.K., McAllister, E., Janssen, B., Mello, S., Avgerinos, E., Pascoe, A.R., Escartin, J., 1997. Corrugated slip surfaces formed at ridge-transform intersections on the Mid-Atlantic Ridge. Nature 385, 329–332.

Cipriani, A., Brueckner, H.K., Bonatti, E., Brunelli, D., 2004. Oceanic crust generated by elusive parents: Sr and Nd isotopes in basalt–peridotite pairs from the Mid-Atlantic Ridge. Geology 32, 657–660.

Cohen, A.S., O'Nions, R.K., Siegenthaler, R., Griffin, W.L., 1988. Chronology of the pressure–temperature history recorded by a granulite terrain. Contrib. Mineral. Petrol. 98, 303–311.

Collins, J.A., Tucholke, B.E., Canales, J.P., 2001. Structure of Mid-Atlantic Ridge megamullions from seismic refraction experiments and multichannel seismic reflection profiling. Eos Trans. AGU, vol. 82. Fall Meet. Suppl., F1100.

Dasch, E.J., Hedge, C.E., Dymond, J., 1973. Effect of seawater interaction on strontium isotope composition of deep-sea basalts. Earth Planet. Sci. Lett. 19, 177–183.

Davis, A.C., Bickle, M.J., Teagle, D.A.H., 2003. Imbalance in the oceanic strontium budget. Earth Planet. Sci. Lett. 211, 173–187.

Delacour, A., 2007. Linking serpentinization, fluid fluxes mass transfer and microbial activity at Lost City: geochemical and isotopic constraints. Ph.D. Thesis No. 17198, ETH Zürich.

Delacour, A., Früh-Green, G.L., Bernasconi, S.M., Kelley, D.S., 2005. The influence of high seawater fluxes on sulfur compositions of the serpentinized peridotites at the Lost City hydrothermal field. Eos Trans. AGU, vol. 86 (52). Fall Meet. Suppl., V51B-1488.

Delacour, A., Früh-Green, G.L., Bernasconi, S.M., Schaeffer, P., Frank, M., Gutjahr, M., Kelley, D.S., 2007. Influence of high fluid fluxes on sulfur and carbon speciation of serpentinites of the Atlantis Massif. Geophys. Res. Abstr. 9, 030907.

Delacour, A., Früh-Green, G.L., Bernasconi, S.M., Schaeffer, P., Frank, M., Gutjahr, M., 2008. Isotopic constraints on seawater-rock interaction and redox conditions of the gabbroic-dominated IODP Hole 1309D, Atlantis Massif (30°N, MAR). Geophys. Res. Abstr. 10 EGU2008-A-08649.

Douville, E., Charlou, J.L., Oelkers, E.H., Bienvenu, P., Jove Colon, C.F., Donval, J.P., Fouquet, Y., Prieur, D., Appriou, P., 2002. The Rainbow vent fluids (36°4'N, MAR): the influence of ultramafic rocks and phase separation on trace metal content in Mid-Atlantic Ridge hydrothermal fluids. Chem. Geol. 184, 37–48.

Drouin, M., Godard, M., Ildefonse, B., 2007. Origin of olivine-rich gabbroic rocks from the Atlantis Massif (MAR 30°N, IODP Hole U1309D): petrostructural and geochemical study. Geophys. Res. Abstr. 9, 06550.

Expedition Scientific Party, 2005a. Oceanic core complex formation, Atlantis Massif, *IODP Prelim. Rept., 304* (online). http://iodp.tamu.edu/publications/PR/304PR/304PR.PDF.

Expedition Scientific Party, 2005b. Oceanic core complex formation, Atlantis Massif, *IODP Prelim. Rept., 305* (online). http://iodp.tamu.edu/publications/PR/305PR/305PR.PDF.

Farrell, J.W., Clemens, S.C., Gromet, L.P., 1995. Improved chronostratigraphic reference curve of Late Neogene seawater $^{87}Sr/^{86}Sr$. Geology 23, 403–406.

Frank, M., van de Flierdt, T., Halliday, A.N., Kubik, P.W., Hattendorf, B., Günther, D., 2003. The evolution of deep water mixing and weathering inputs in the central Atlantic Ocean over the past 33 Myr. Paleoceanography 18, 1091. doi:10.1029/2003PA000919.

Früh-Green, G.L., Kelley, D.S., Bernasconi, S.M., Karson, J.A., Ludwig, K.A., Butterfield, D.A., Boschi, C., Proskurowski, G., 2003. 30,000 years of hydrothermal activity at the Lost City vent field. Science 301, 495–498.

Früh-Green, G.L., Connolly, J.A.D., Plas, A., Kelley, D.S., Grobéty, B., 2004. Serpentinization of oceanic peridotites: implications for geochemical cycles and biological activity. In: Wilcock, W.S.D., et al. (Ed.), The subseafloor biosphere at mid-ocean ridges. Geophys. Monogr. Ser., vol. 144. American Geophysical Union, Washington, D. C., pp. 119–136.

Früh-Green, G.L., Boschi, C., Kelley, D.S., Delacour, A., Bernasconi, S.M., Karson, J.A., 2005. Insights into peridotite-hosted hydrothermal systems from petrological and geochemical studies of the Lost City hydrothermal system. Eos Trans. AGU, vol. 86(52). Fall Meet. Suppl., V43C-03.

Gao, Y., Hoefs, J., Przybilla, R., Snow, J.E., 2006. A complete oxygen isotope profile through the lower oceanic crust, ODP Hole 735B. Chem. Geol. 233, 217–234.

Gillis, K.M., Ludden, J.N., Smith, A.D., 1992. Mobilization of REE during crustal aging in the Troodos Ophiolite, Cyprus. Chem. Geol. 98, 71–86.

Gillis, K.M., Coogan, L.A., Pedersen, R., 2005. Strontium isotope constraints on fluid flow in the upper oceanic crust at the East Pacific Rise. Earth Planet. Sci. Lett. 232, 83–94.

Grauch, R.I., 1989. Rare earth elements in metamorphic rocks. In: Lipin, B.R., McKay, G.A. (Eds.), Geochemistry and Mineralogy of rare earth elements. . Rev. Mineral. Geoch., vol. 21. Mineralogical Society of America, Washington, D. C., pp. 147–167.

Hart, R., 1970. Chemical exchange between seawater and deep ocean basalts. Earth Planet. Sci. Lett. 9, 269–279.

Hart, S.R., Erlank, A.J., Kable, E.D.J., 1974. Sea floor basalt alteration: some chemical and Sr isotopic effects. Contrib. Mineral. Petrol. 44, 219–230.

Hart, S.R., Blusztajn, J.S., Dick, H.J.B., Meyer, P.S., Muehlenbachs, K., 1999. The fingerprint of seawater circulation in a 500-meter section of ocean crust gabbros. Geochim. Cosmochim. Acta 63, 4059–4080.

Hess, J., Bender, M., Schilling, J.G., 1991. Assessing seawater/basalt exchange of strontium isotopes in hydrothermal processes on the flanks of mid-ocean ridges. Earth Planet. Sci. Lett. 103, 133–142.

Holm, P.M., 2002. Sr, Nd and Pb isotopic composition of in situ lower crust at the Southwest Indian Ridge: results from ODP Leg 176. Chem. Geol. 184, 195–216.

Horwitz, E.P., Chiarizia, R., Dietz, M.L., 1992. A novel strontium-selective extraction chromatographic resin. Solv. Extr. Ion Exch. 10, 313–336.

Humphris, S.E., 1984. The mobility of rare earth elements in the crust. In: Henderson, P. (Ed.), Rare earth element geochemistry, pp. 317–342.

Humphris, S.E., Thompson, G., 1978a. Hydrothermal alteration of oceanic basalts by seawater. Geochim. Cosmochim. Acta 42, 107–125.

Humphris, S.E., Thompson, G., 1978b. Trace element mobility during hydrothermal alteration of oceanic basalts. Geochim. Cosmochim. Acta 42, 127–136.

Ildefonse, B., Blackman, D., John, B.E., Ohara, Y., Miller, D.J., MacLeod, C.J., IODP Expeditions 304/305 Science Party, 2007. Oceanic core complexes and crustal accretion at slow-spreading ridges. Geology 35, 623–626.

Jacobsen, S.B., Wasserburg, G.J., 1979. Nd and Sr isotopic study of the Bay of Islands ophiolitic complex and the evolution of the source of the midocean ridge basalts. J. Geophys. Res. 84, 7429–7445.

Jacobsen, S.B., Wasserburg, G.J., 1980. Sm–Nd isotopic evolution of chondrites. Earth Planet. Sci. Lett. 50, 139–155.

Kakihana, H., Kotaka, M., Shohei, S., Nomura, M., Okamoto, N., 1977. Fundamental studies on ion-exchange separation of boron isotopes. Bull. Chem. Soc. Jpn. 50, 158–163.

Karson, J.A., 1998. Internal structure of oceanice lithosphere: a perspective from tectonic windows. In: Buck, et al. (Ed.), Faulting and Magmatism at Mid-Ocean Ridges. Geophys. Monogr. Ser., vol. 106. American Geophysical Union, Washington, D. C., pp. 177–218.

Karson, J.A., Früh-Green, G.L., Kelley, D.S., Williams, E.A., Yoerger, D.R., Jakuba, M., 2006. Detachment shear zone of the Atlantis Massif core complex, Mid-Atlantic Ridge, 30°N. Geochem. Geophys. Geosyst. 7, Q06016. doi:10.1029/2005GC001109.

Kawahata, H., Scott, S.D., 1990. Strontium isotopes and water–rock interaction of the Agrokipia 'B' stockwork deposit in the Troodos ophiolite, Cyprus: a fossil subseafloor ore body. Geochem. J. 24, 349–356.

Kelley, D.S., Karson, J.A., Blackman, D.K., Früh-Green, G.L., Butterfield, D.A., Lilley, M.D., Olson, E.J., Schrenk, M.O., Roe, K.K., Lebon, G.T., Rivizzigno, P., Scientific Party, 2001. An off-axis hydrothermal vent field near the Mid-Atlantic Ridge at 30°N. Nature 412, 145–149.

Kelley, D.S., Karson, J.A., Früh-Green, G.L., Yoerger, D.R., Shank, T.M., Butterfield, D.A., Hayes, J.M., Schrenk, M.O., Olson, E.J., Proskurowski, G., Jakuba, M., Bradley, A., Larson, B., Ludwig, K., Glickson, D., Buckman, K., Bradley, A.S., Brazelton, W.J., Roe, K., Elend, M.J., Delacour, A., Bernasconi, S.M., Lilley, M.D., Baross, J.A., Summons, R.E., Sylva, S., 2005. A serpentinite-hosted ecosystem: the Lost City hydrothermal field. Science 307, 1428–1434.

Kempton, P.D., Hunter, A.G., 1997. A Sr-, Nd-, Pb-, O-isotope study of plutonic rocks from MARK, leg 153: implications for mantle heterogeneity and magma chamber processes. Proc. Ocean Drill. Program Sci. Results 153, 305–319.

Kempton, P.D., Stephens, C.J., 1997. Petrology and geochemistry of nodular websterite inclusions in harzburgite, Hole 920D. Proc. Ocean Drill. Program Sci. Results 153, 321–3312.

Kempton, P.D., Hawkesworth, C.J., Fowler, M., 1991. Geochemistry and isotopic composition of gabbros from layer 3 of the Indian ocean crust, Hole 735B. Proc. Ocean Drill. Program Sci. Results 118, 127–143.

Lagabrielle, Y., Bideau, D., Cannat, M., Karson, J.A., Mével, C., 1998. Ultramafic-, mafic plutonic rock suites exposed along the Mid-Atlantic Ridge (10°N–30°N). Symmetrical–Asymmetrical distribution and implications for seafloor spreading processes. In: Buck, et al. (Ed.), Faulting and Magmatism at Mid-Ocean Ridges. Geophys. Monogr. Ser., vol. 106. AGU, Washington, D. C., pp. 153–176.

Leblanc, M., Lbouabi, M., 1988. Native silver mineralization along a rodingite tectonic contact between serpentinite and quartz diorite (Bou Azzer, Morocco). Econ. Geol. 83, 1379–1391.

Ludden, J.N., Thompson, G., 1979. An evaluation of the behavior of the rare earth elements during the weathering of sea-floor basalt. Earth Planet. Sci. Lett. 43, 85–92.

Ludwig, K.A., Kelley, D.S., Edwards, R.L., Shen, C.-C., Cheng, H., 2005. U/Th geochronology of carbonate chimneys at the Lost City hydrothermal field. Eos Trans. AGU, vol. 86 (52). Fall Meet. Suppl., V51B-1487.

Ludwig, K., Kelley, D.S., Butterfield, D.A., Nelson, B.K., Früh-Green, G.L., 2006. Formation and evolution of carbonate chimneys at the Lost City hydrothermal field. Geochim. Cosmochim. Acta 70, 3625–3645.

McCulloch, M.T., Gregory, R.T., Wasserburg, G.J., Taylor, H.P.J., 1980. A neodymium, strontium, and oxygen isotopic study of the Cretaceous Samail ophiolite and implications for the petrogenesis and seawater-hydrothermal alteration of oceanic crust. Earth Planet. Sci. Lett. 46, 201–211.

McDonough, W.F., Sun, S.S., 1995. The composition of the Earth. Chem. Geol. 120, 223–253.

Menzies, M., Seyfried, W.E.J., 1979. Basalt–seawater interaction trace element and strontium isotopic variations in experimentally altered glassy basalt. Earth Planet. Sci. Lett. 44, 463–472.
Menzies, M., Long, A., Ingram, G., Tatnell, M., Janecky, D.R., 1993. MORB peridotite–seawater interaction: experimental constraints on the behaviour of trace elements, $^{87}Sr/^{86}Sr$ and $^{143}Nd/^{144}Nd$ ratios. In: Prichard, H.M., Alabaster, T., Harris, N.B.W., Neary, C.R. (Eds.), Magmatic processes and plate tectonics. Geol. Soc. Spec. Pub., vol. 76, pp. 309–322.
Mével, C., 2003. Serpentinization of abyssal peridotites at mid-ocean ridges. C. R. Geosci. 335, 825–852.
Michard, A., Albarède, F., 1986. The REE content of some hydrothermal fluids. Chem. Geol. 55, 51–60.
Michard, A., Albarède, F., Minster, J.F., Charlou, J.-L., 1983. Rare-earth elements and uranium in high temperature solutions from the East Pacific Rise hydrothermal vent field (13°N). Nature 303, 795–797.
Négrel, P., Guerrot, C., Cocherie, A., Azaroual, M., Brach, M., Fouillac, C., 2000. Rare earth elements, neodymium and strontium isotopic systematics in mineral waters: evidence from the Massif Central, France. Appl. Geochem. 15, 1345–1367.
Nesbitt, H.W., 1979. Mobility and fractionation of rare earth elements during weathering of a granodiorite. Nature 279, 207–210.
Nier, A.O., 1938. The isotopic constitution of strontium, barium, bismuth, thallium and mercury. Phys. Rev. 54, 275–278.
O'Hanley, D.S., 1996. Serpentinites: Record of Tectonic and Petrological History. Oxford Univ. Press, New York. 277 pp.
O'Nions, R.K., Frank, M., von Blanckenburg, F., Ling, H.-F., 1998. Secular variation of Nd and Pb isotopes in ferromanganese crusts from the Atlantic, Indian and Pacific Oceans. Earth Planet. Sci. Lett. 155, 15–28.
Palmer, M.R., Edmond, J.M., 1989. The strontium isotope budget of the modern ocean Earth Planet. Sci. Lett. 92, 11–26.
Palmer, M.R., Swihart, G.H., 1996. Boron isotope geochemistry; an overview. In: Grew, E.S., Anovitz, L.M. (Eds.), Boron; Mineralogy, Petrology and Geochemistry. Rev. Mineral. Geoch., vol. 33. Mineralogical Society of America, Washington, D. C., pp. 709–744.
Paulick, H., Bach, W., Godard, M., De Hoog, J.C.M., Suhr, G., Harvey, J., 2006. Geochemistry of abyssal peridotites (Mid-Atlantic Ridge, 15°20′N, ODP Leg 209): implications for fluid/rock interaction in slow spreading environments. Chem. Geol. 234, 179–210.
Piepgras, D.J., Wasserburg, G.J., 1980. Neodymium isotopic variations in seawater. Earth Planet. Sci. Lett. 50, 128–138.
Piepgras, D.J., Wasserburg, G.J., 1987. Rare-earth element transport in the western North-Atlantic inferred from Nd isotopic observations. Geochim. Cosmochim. Acta 51, 1257–1271.
Piepgras, D.J., Wasserburg, G.J., Dasch, E.J., 1979. The isotopic composition of Nd in different ocean masses. Earth Planet. Sci. Lett. 45, 223–236.
Plank, T., Langmuir, C.H., 1998. The chemical composition of subducting sediment and its consequences for the crust and mantle. Chem. Geol. 145, 325–394.
Poitrasson, F., Pin, C., Duthou, J.L., 1995. Hydrothermal remobilization of rare earth elements and its effect on Nd isotopes in rhyolite and granite. Earth Planet. Sci. Lett. 130, 1–11.
Proskurowski, G., Lilley, M.D., Kelley, D.S., Olson, E.J., 2006. Low temperature volatile production at the Lost City hydrothermal field, evidence from a hydrogen stable isotope geothermometer. Chem. Geol. 229, 331–343.
Reynolds, B.C., Frank, M., O'Nions, R.K., 1999. Nd- and Pb- isotope time series from Atlantic ferromanganese crusts: implications for changes in provenance and paleocirculation over the last 8 Myr. Earth Planet. Sci. Lett. 173, 381–396.
Salters, V.J.M., Dick, H.J.B., 2002. Mineralogy of the mid-ocean ridge basalt source from neodymium isotopic composition of abyssal peridotites. Nature 418, 68–72.
Schrenk, M.O., Kelley, D.S., Bolton, S.A., Baross, J.A., 2004. Low Archaeal diversity linked to subseafloor geochemical processes at the Lost City hydrothermal field, Mid-Atlantic Ridge. Environ. Microbiol. 6, 1086–1095.
Schroeder, T., John, B.E., 2004. Strain localization on an oceanic detachment fault system, Atlantis Massif, 30°N, Mid-Atlantic Ridge. Geochem. Geophys. Geosyst. 5. doi:10.1029/2004GC000728.
Snow, J.E., Dick, H.J.B., 1995. Pervasive magnesium loss by marine weathering of peridotite. Geochim. Cosmochim. Acta 59, 4219–4235.
Snow, J.E., Hart, S.R., Dick, H.J.B., 1994. Nd and Sr isotope evidence linking mid-ocean ridge basalts and abyssal peridotites. Nature 371, 57–60.
Spooner, E.T.C., Chapman, H.J., Smewing, J.D., 1977. Strontium isotopic contamination and oxidation during ocean floor hydrothermal metamorphism of the ophiolitic rocks of the Troodos Massif, Cyprus. Geochim. Cosmochim. Acta 41, 873–890.
Stakes, D., Mével, C., Cannat, M., Chaput, T., 1991. Metamorphic stratigraphy of Hole 735B. Proc. Ocean Drill. Program Sci. Results 118, 153–180.
Steiger, R.H., Jager, E., 1977. Subcommission on geochronology: convention on the use of decay constants in geo- and cosmochronology. Earth Planet. Sci. Lett. 36, 359–362.
Sun, S.S., McDonough, W.F., 1989. Chemical and isotopic systematics of oceanic basalts: implications for mantle composition and processes. In: Saunders, A.D., Norry, M.J. (Eds.), Magmatism in the Ocean Basins. Geol. Soc. London Spec. Publ, vol. 42, pp. 313–345.
Sverjensky, D.A., 1984. Europium redox equilibria in aqueous solution. Earth Planet. Sci. Lett. 67, 70–78.
Tachikawa, K., Jeandel, C., Roy-Barman, M., 1999. A new approach to the Nd residence time in the ocean: the role of atmospheric inputs. Earth Planet. Sci. Lett. 170, 433–446.
Tanaka, T., Togashi, S., Kamioka, H., Amakawa, H., Kagami, H., Hamamoto, T., Yuhara, M., Orihashi, Y., Yoneda, S., Shimizu, H., Kunimaru, T., Takahashi, K., Yanagi, T., Nakano, T., Fujimaki, H., Shinjo, R., Asahara, Y., Tanimizu, M., Dragusanu, C., 2000. JNdi-1: a neodymium isotopic reference in consistency with LaJolla neodymium. Chem. Geol. 168, 279–281.
Taylor, H.P.J., 1977. Water/rock interactions and the origin of H_2O in granitic batholiths. J. Geol. Soc. (Lond.) 133, 509–558.
Teagle, D.A.H., Bickle, M.J., Alt, J.C., 2003. Recharge flux to ocean ridge black smoker systems: a geochemical estimate from ODP Home 504B Earth Planet. Sci. Lett. 210, 81–89.
Workman, R.K., Hart, S.R., 2005. Major and trace element composition of the depleted MORB mantle (DMM). Earth Planet. Sci. Lett. 231, 53–72.